887.

A STUDY OF PRESSURE SOLUTION EFFECTS

A STUDY OF PRESSURE SOLUTION EFFECTS

By

FRANK FUETEN

A Thesis

Submitted to the Faculty of Science

in Partial Fulfilment of the Requirements

for the Degree

Bachelor of Science

McMaster University

April, 1982

HONOURS BACHELOR OF SCIENCE (1982)
(Geology)

McMASTER UNIVERSITY
Hamilton, Ontario

TITLE: A Study of Pressure Solution Effects

AUTHOR: Frank Fueten

SUPERVISOR: Dr. P.M. Clifford

NUMBER OF PAGES: vii, 68

To My Parents

Abstract

A microscopic study of two samples of the Gowganda Formation, both having undergone pure shear deformation at greenschist facies metamorphism has shown:

Sample A - Reduction in quartz grain size, and pressure solution shadows were evidence for strong pressure solution activity. Pre-lithification fractures provided channelways for the removal of quartz and water out of the system. Matrix quartz was not recrystallized.

Sample B - Extensive local recrystallization of quartz due to pressure solution activity caused metamorphic segregation and the formation of a cleavage. Cleavage behaviour differs in the matrix from that observed in an area of contact strain, as produced by a buckled quartz vein. There is no evidence for removal of quartz from the system.

A comparison between the two samples suggests that (a) water, in this case at least, is necessary to produce metamorphic segregation, (b) the system has to be closed to reach metamorphic segregation and (c) original features may be preserved through limited metamorphism if the rock is dried out early in its history.

Acknowledgments

I am greatly indebted to Dr. P.M. Clifford, my thesis supervisor, for all his help, especially for his continuous patient attempts to introduce me to the use of the English language. Thank you also to Dr. P.F. Robin, who made many helpful suggestions. I would also like to thank Andy Fyon for helping me in various ways. Len Zwicker's skill for preparing excellent thin sections is greatly appreciated. Many thanks are extended to Jack Whorwood, for his expert photography. I would also like to thank Libby Ginn; without her ability to read my scrawl, typing skills and other help, this thesis would still be on scrap paper.

And then of course, there are my friends. You have made this year, as the previous ones, very enjoyable for me. Thanx guys. Finally I would sincerely like to thank my family and Belinda Henry, who in one way or another, are to a high degree responsible for what I turned out to be.

TABLE OF CONTENTS

LIST OF FIGURES

CHAPTER 1

1.1 Introduction

This study looks in detail at two types of cleavages. Specimens used are from the same Formation and are therefore of approximately the same age. They are also at roughly the same metamorphic grade.

There are, however, fundamental differences in the cleavages which they contain. Sample A displays a cleavage that appears well developed on the outcrop scale, but is not at all apparent on the thin section scale. The cleavage in sample B is well developed at both microscopic and outcrop scale.

The cleavage in both cases is thought to have developed under an essentially pure shear regime. This study will restrict itself to viewing processes leading to the cleavage development, in two dimensions. The plane of study is perpendicular to the cleavage plane. It is assumed that all significant processes take place in this plane and are merely repeated as one goes down dip of the cleavage. A similar assumption was made and justified by Ramsay and Graham (1970).

1.2 Previous Work

Pressure solution, first described and discussed by Sorby in limestone in 1863, deals with the dissolution of minerals under non-hydrostatic stress. Pressure solution may lead to stylolite formation and compaction or to indentation and welding of granular material. It may occur in limestones, dolomites and sandstones (Durney, 1972). Trurnit (1968) summarizes the effects of pressure solution by means of 14 pressure solution contacts (Figure 1.1). Alvarez et al. (1978) and Engelder et al. (1979) describe pressure solution in limestones, where it is responsible for the formation of a cleavage and may be responsible for the removal of material producing a shortening of beds of up to 50%. Pressure solution may remove calcite or quartz in greywackes (Beach, 1974). The material removed may be redeposited in veins, either locally or distally.

Pressure solution in general, therefore, involves local rearrangement of mass, or absolute removal of material, with associated volume loss. Several authors, example Cosgrove (1974), regard it as part of the process which yields cleavage.

The processes leading to metamorphic segregation are still not well understood. Diffusion controlled by some sort of gradients in pressure or mean pressure is thought to cause and or control this mechanism (Durney, 1972). The

Figure 1.1 The fourteen pressure solution contacts with contact formulas (after Trurnit, 1968)

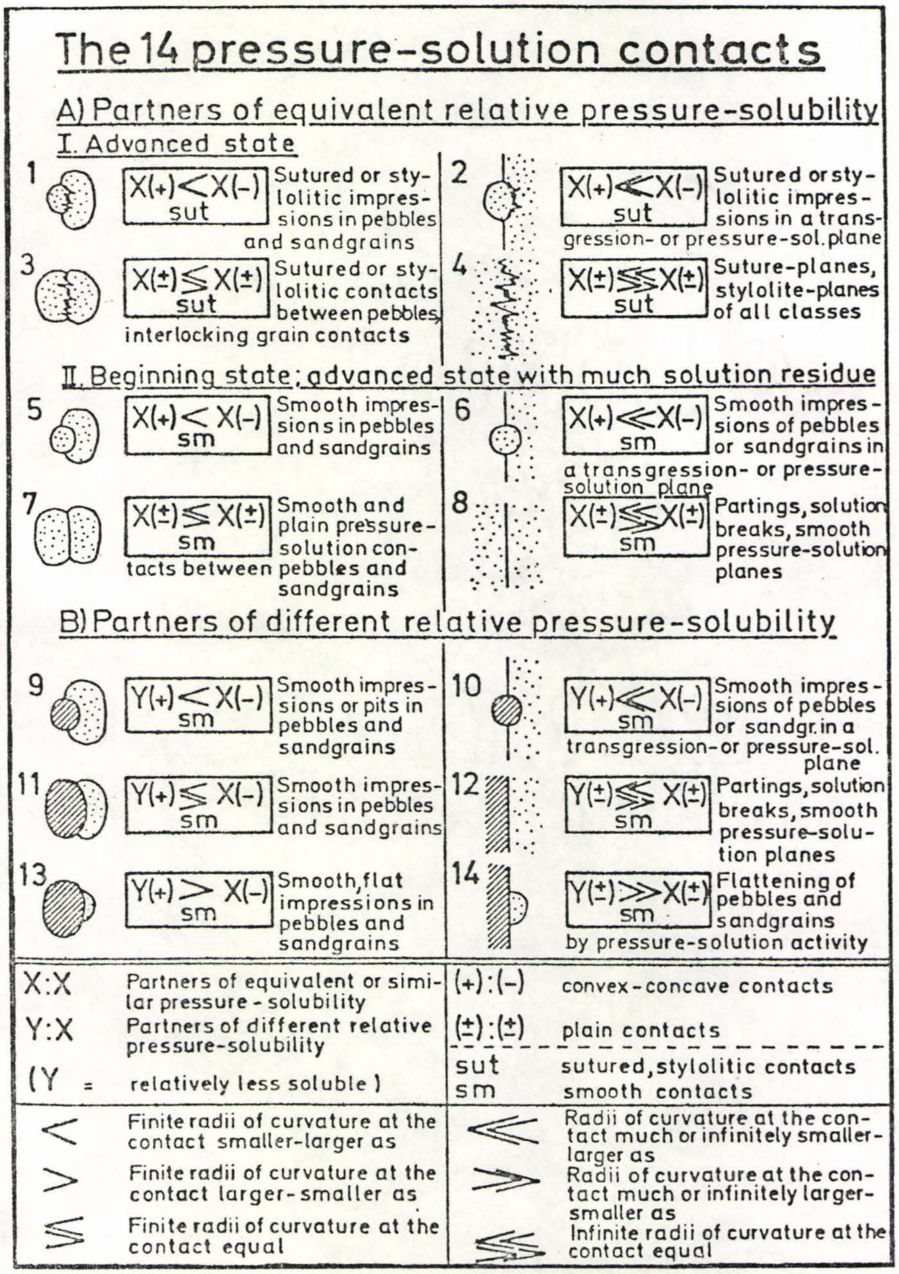
The 14 pressure-solution contacts
A) Partners of equivalent relative pressure-solubility
I. Advanced state
1
X(+) < X(-) sut
Sutured or stylolitic impressions in pebbles and sandgrains
2
X(+) ≪ X(-) sut
Sutured or stylolitic impressions in a transgression- or pressure-sol. plane
3
X(±) ≶ X(±) sut
Sutured or stylolitic contacts between pebbles, interlocking grain contacts
4
X(±) ⋚ X(±) sut
Suture-planes, stylolite-planes of all classes
II. Beginning state; advanced state with much solution residue
5
X(+) < X(-) sm
Smooth impressions in pebbles and sandgrains
6
X(+) ≪ X(-) sm
Smooth impressions of pebbles or sandgrains in a transgression- or pressure-solution plane
7
X(±) ≶ X(±) sm
Smooth and plain pressure-solution contacts between pebbles and sandgrains
8
X(±) ⋚ X(±) sm
Partings, solution breaks, smooth pressure-solution planes
B) Partners of different relative pressure-solubility
9
Y(+) < X(-) sm
Smooth impressions or pits in pebbles and sandgrains
10
Y(+) ≪ X(-) sm
Smooth impressions of pebbles or sandgr. in a transgression- or pressure-sol. plane
11
Y(+) ≶ X(-) sm
Smooth impressions in pebbles and sandgrains
12
Y(±) ⋚ X(±) sm
Partings, solution breaks, smooth pressure-solution planes
13
Y(+) > X(-) sm
Smooth, flat impressions in pebbles and sandgrains
14
Y(±) ≫ X(±) sm
Flattening of pebbles and sandgrains by pressure-solution activity
X:X Partners of equivalent or similar pressure-solubility
Y:X Partners of different relative pressure-solubility
(Y = relatively less soluble)
(+):(-) convex-concave contacts
(±):(±) plain contacts
sut sutured, stylolitic contacts
sm smooth contacts
< Finite radii of curvature at the contact smaller-larger as
> Finite radii of curvature at the contact larger-smaller as
≶ Finite radii of curvature at the contact equal
≪ Radii of curvature at the contact much or infinitely smaller-larger as
≫ Radii of curvature at the contact much or infinitely larger-smaller as
⋚ Infinite radii of curvature at the contact equal

exact origin or nature of these gradients is not known though.

On the basis of petrographic observations (Gray, 1978, Hobbs <u>et al</u>., 1976) it seems that silica is the most mobile component. Robin (1979) proposes that micas, in a quartz-mica rock, act as a catalyst in the segregation. This implies that rocks consisting of almost pure quartz and almost pure mica are competent. Between the two end members of the systems competency is as shown in figure 1.2 . The position of the minimum is dependent on a number of factors such as differential stress, temperature, chemical potential and abundance of water, grain size, etc.

1.3 Location

Both specimens are from the Gowganda Formation, the lower Member of the Cobalt Group, which is part of the Huronian Supergroup. The age of the formation is quoted as 2.2-2.5 By. (Robertson, 1976). The metamorphic grade ranges from greenschist to amphibolite facies (Robertson, 1976) within this formation. Samples A and B have undergone greenschist facies metamorphism.

Sample A was collected from a road outcrop approximately 10 km north of Whitefish Falls on highway #68.

Sample B was collected by Dr. P.M. Clifford. Sample B is a piece of float, but is from the Bruce Formation as

Figure 1.2 Competency as a function of mica/quartz ratio, as expected if the deformation rate were controlled by the diffusion of silica catalysed by micas. Rocks with little or no micas are competent because of restricted diffusion paths. Rocks with little or no quartz are competent because chemical components of micas are less 'mobile' than silica, and micas are therefore more resistant to pressure-induced diffusion transfer. The 'normal' relationship, that of decreasing competency with increasing mica content (left-hand side of curve), explains why segregation develops. The minimum in the curves accounts for the lack of apparent compentency contrast between some 'equilibrium' bands in the field.

(after Robin, 1979)

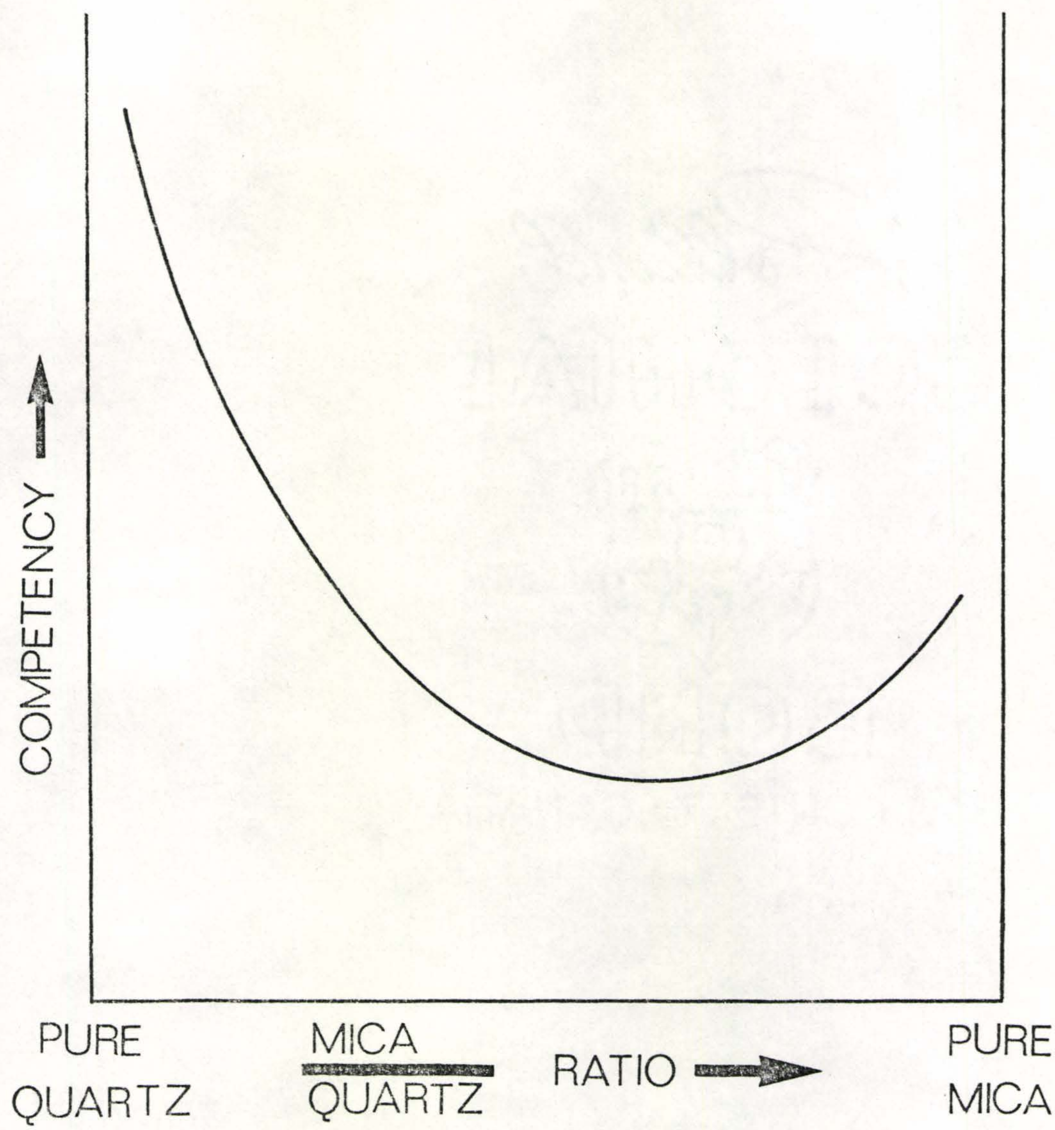
COMPETENCY
PURE
QUARTZ
MICA
QUARTZ
RATIO
PURE
MICA

exposed on a small headland about 1.4 km due southeast of Whitefish Falls on the north shore of lake Huron.

For more information on the regional geology refer to James A. Robertson (1976) or the Geol. Guide Book #4, Ontario Division of Mines.

1.4 Temperature and Pressure Limits

The mineral assemblages of the samples are given in figure 1.3. Both samples can be classified as metagraywackes. The lower boundary of their metamorphic grade is given by the reaction leading to the appearance of the assemblage: biotite + muscovite. This reaction takes place at just over $400^{o}C$. The upper limit of the metamorphic temperature change for these samples is approximately $500^{o}C$ and is determined by disappearance of chlorite and muscovite. The temperatures for both reactions do not vary significantly over a wide range of pressures. Since biotite, muscovite and chlorite are present in both samples, the metamorphic temperature for these samples has to be between 400^{o} and $500^{o}C$.

The pressure cannot be determined at all accurately. A maximum pressure is given by the conversion of calcite to aragonite, which at this temperature range takes place at pressures of about 9 kb. Since the samples contain calcite pressure obviously did not exceed 9 kb; no tighter limits

Figure 1.3 Bulk composition of samples A and B.

Sample A		Sample B	
Quartz	- 54%	Quartz	- 42%
Albite	- 25%	Chlorite	- 15%
Calcite	- 10%	Muscovite	- 15%
Biotite	- 3%	Biotite	- 12%
Chlorite	- 3%	Epidote	- 5%
Sericite	- 3%	Albite	- 3%
Epidote	- 2%	Opaques	- 8%
Opaques	- trace 1%		

can be given.

The metamorphic grade of these samples is that of greenschist facies.

CHAPTER 2

2.1 Sample A - Description

The unit from which sample A was taken is cut by two breccia zones, usually referred to as Sudbury breccia. These zones are broadly parallel to the cleavage, which has an orientation of $065^{\circ}/75^{\circ}$ N. Two prominent joint sets have orientations of $170^{\circ}/80^{\circ}$N and $030^{\circ}/12^{\circ}$S.

The unit contains large quantities of rock fragments of various compositions and sizes. The most abundant rock fragments are of quartzite. The size of the rock fragments ranges from 1 mm to 10-15 cm in diameter and their shape ranges from angular to well rounded. The grain size of the matrix is approximately 0.01-0.05 mm.

Some fragments have been tensionally fractured and extended, with calcite filling the fractures. The fractured fragments are up to about 5 cm in diameter. No fractured pebbles above calculated original diameter of 5 cm have been observed. This assumes constant volume.

Other than the joint sets, no systematic fractures are observed with the naked eye. In the thin section, however, one can see that the rock is highly fractured on the microscopic scale. The fracture density varies from slide to slide, ranging from 2 to 10 fractures per cm^2.

These fractures can easily be recognized since they are filled with mica. In some fractures the micas are oriented parallel to the fractures. In other fractures the micas show a preferred alignment perpendicular to the fractures, or they may be totally unoriented. Inequant clasts show no preferred overall orientation; there are so few that it is unprofitable to attempt an orientation analysis.

The matrix is made up of angular to well rounded grains. The majority of quartz shows undulatory extinction. Feldspar and calcite exhibit twinning. There is no differentiation into quartz and mica rich layers in this sample.

2.2 Detailed Description

Slide F07-1

Slide F07-1, figure 2.1, exhibits a high fracture density. The most prominent thing in this slide is the large fracture running straight across the slide. This "master" fracture is actually a bundle of several parallel, closely spaced, fractures. This bundle is composed of one major continuous fracture, flanked by a large number of fractures, which are mainly discontinuous. Into this "master" fracture lead a large number of smaller, thinner "feeder" fractures. These small "feeder" fractures approach the "master" obliquely, usually at an angle of less than 45°.

Figure 2.1 Slide F07-1. Polarized photograph on top and point light source photograph on the bottom. A "master" fracture, with and east-west orientation, is approached by "feeder" fractures at predominantly low angles. A gradual decrease of average grain size towards the center of the slide can best be seen in the polarized photograph.

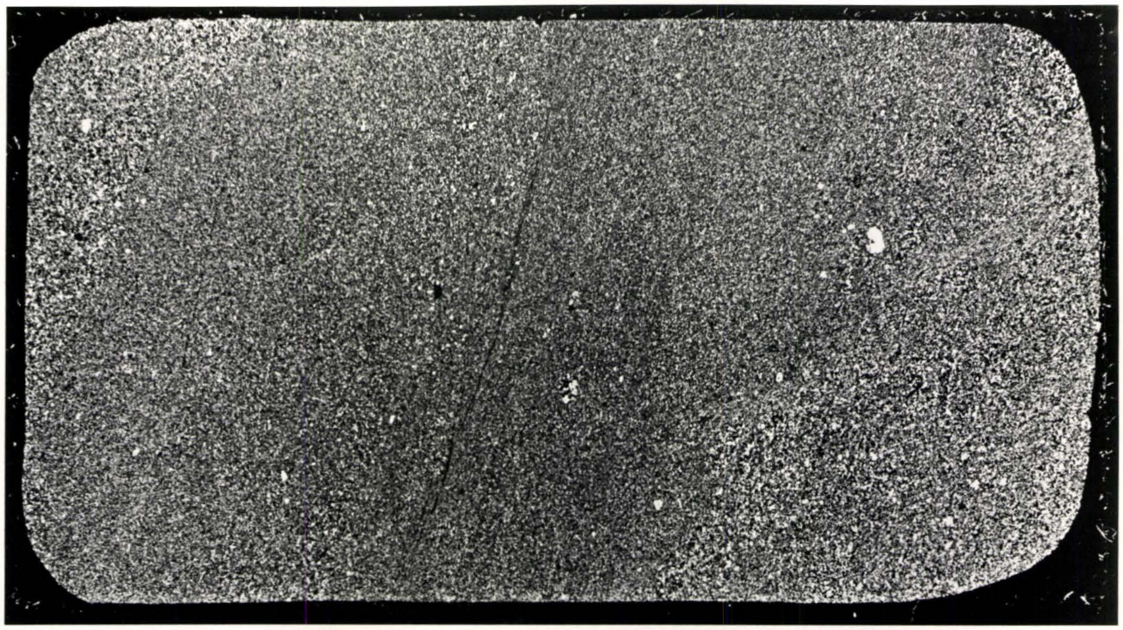

→ N

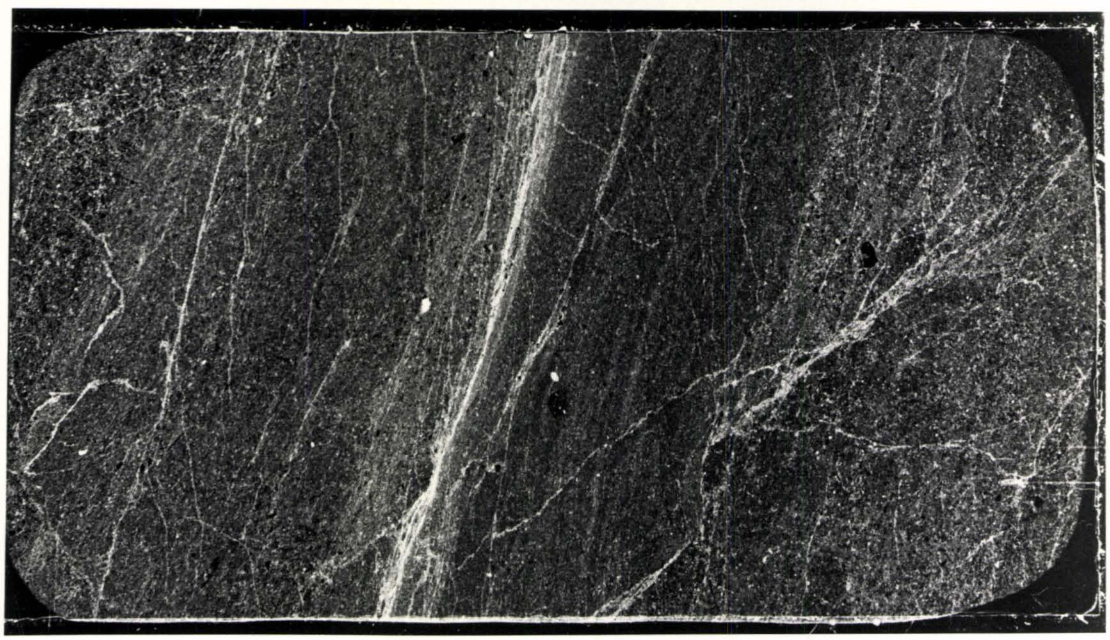

There is a marked decrease in grain size with decreasing distance from the "master" fracture. Two distinct stages are present in this decrease. Taking the grain size at the northeast edge of the slide as a standard grain size then the middle area of the slide, with the exception of the immediate area of the "master" fracture, represents a field of gradational grain size decrease, by a factor of 0.5 to 0.3 of the standard grain size. In the immediate area of the "master" fracture a sharp decrease in grain size down to 0.25-0.20 of the standard grain size is observed. This variation in grain size cannot be mistaken for bedding, because it is totally unlike bedding seen in other sections.

Slide F03

Slide F03, figure 2.2, contains a small vein, filled mostly with calcite, which also contains 20% quartz of larger grain size than the matrix. The quartz in the vein is strained and the calcites show up to two oblique twin sets. This vein is offset in an east-west direction along fractures.

A zone of fractures, about 3 mm wide runs through the slide in a northeast-southwest direction. In this zone a number of fracture-bounded blocks have rhombic outlines. The long diagonal of the rhombs are roughly parallel to the orientation of the fracture zone.

Figure 2.2 Slide F03. Polarized photograph on top and point light source photograph on the bottom. Pressure solution shadows are present on the north-south edges of the clasts. A zone of fractures, with an approximate orientation of northwest-southeast outlines rhombic blocks. A vein is offset along fractures.

N

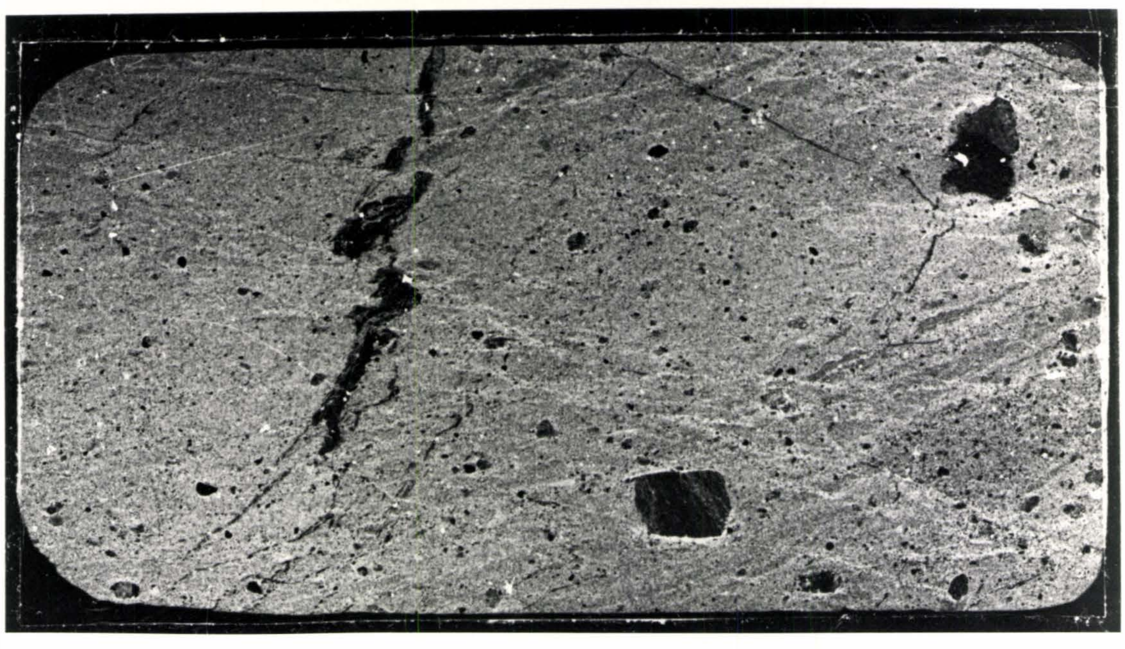

The clasts in this slide show enrichment of micas along their north and south edges, which are called pressure solution shadows. There is no enrichment of quartz on the east and west sides of the clasts.

Slide F07-4

Slide F07-4, figure 2.3, shows a high fracture density. A large "master" fracture runs through the slide roughly in a northeast-southwest direction. The "master" fracture in this slide is a single large fracture, which contains quartz grains. This quartz is of larger grain size than the average quartz grain size in the matrix; it also exhibits subgraining, mosaic grain boundaries, inclusions and undulatory extinction.

Also present are "feeder" fractures which join the "master" fracture. These "feeder" fractures often approach the "master" fractures at high angles of up to 90°. There is no overall gradual decrease in grain size as was observed in F07-1. However, between the "master" and the "feeder" fractures there is a diffuse zone of strong mica enrichment, especially where a large "feeder" fracture joins the "master" fracture.

There is a probable shear displacement along the fracture. A coarser grained, roughly east-west oriented layer approaches the fracture on the east side, but is not present on the west side.

Figure 2.3 Slide F07-4. Polarized photograph on top and point light source photograph on the bottom. A "master" fracture running roughly north-south with "feeder" fractures approaching it at high angles. Areas of pressure solution activity are located at "master-feeder" fracture intersections. Correlatable coarse grained layers are discontinued across the "feeder" fracture.

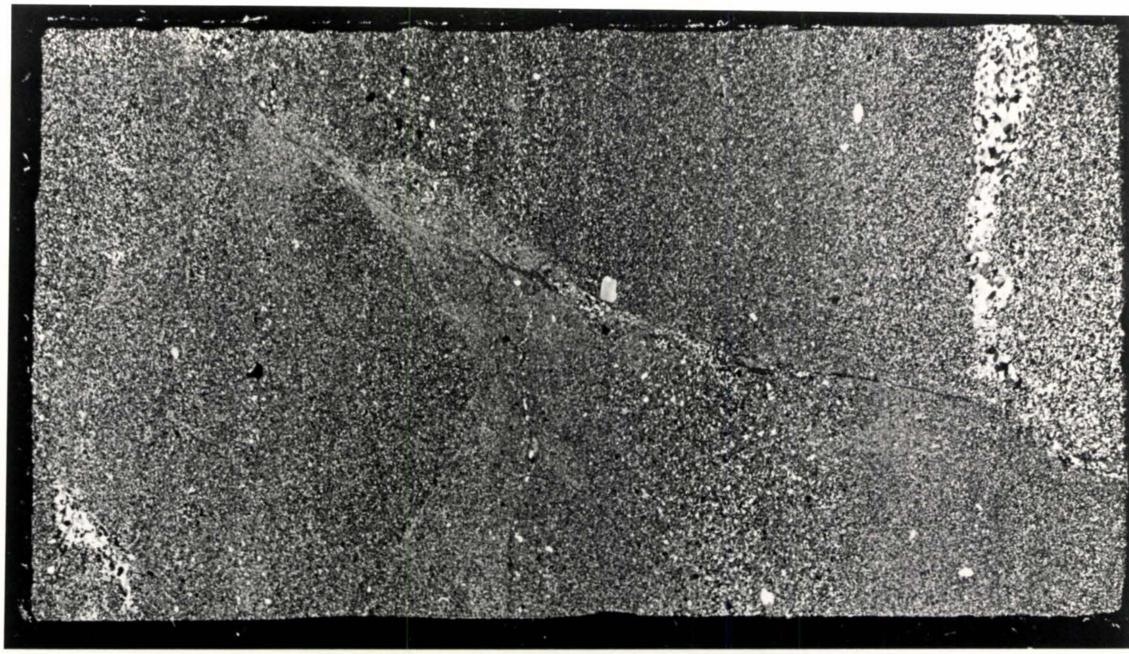

→ N

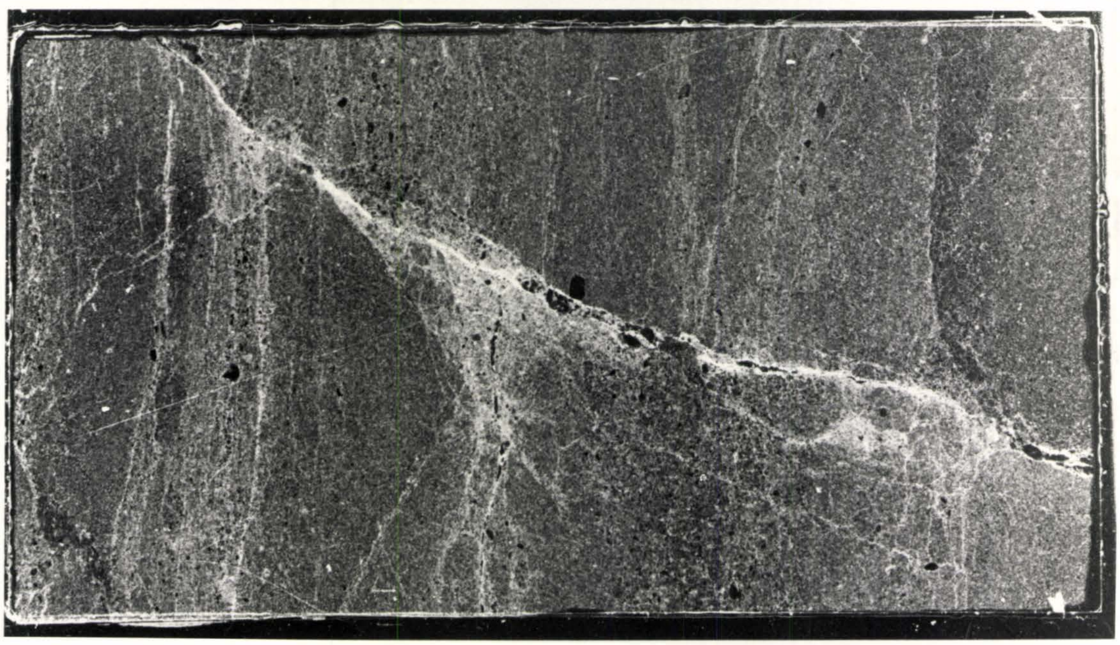

Slide F011

The grain size in slide F011, figure 2.4, is overall slightly less than in the other slides, there is however, a coarser grained layer; presumably bedding, which has an orientation of grains in the matrix which is developed more strongly than in other sections. Fracture density is low in this slide. The fractures present are long and thin and show a preferred orientation of about 100^{o}. The coarser grained layer is offset along fractures in an east-west direction by amounts of up to 1.5 mm. Coarse grains in this layer are flattened adjacent to a fracture.

Other slides

All other slides have intermediate fracture densities. Slides F06, F08-1B, F08-2B, F07-3, show enrichment of micas on the north and south edges of clasts. No enrichment of quartz is found on the east-west edges of clasts.

2.3 Fractures

The fractures displayed in sample A may be a useful tool in determining the strain this rock has undergone. In order for the fractures to be useful, two conditions have to be met:

1) The initial distribution of the fractures had to be random and

→ N

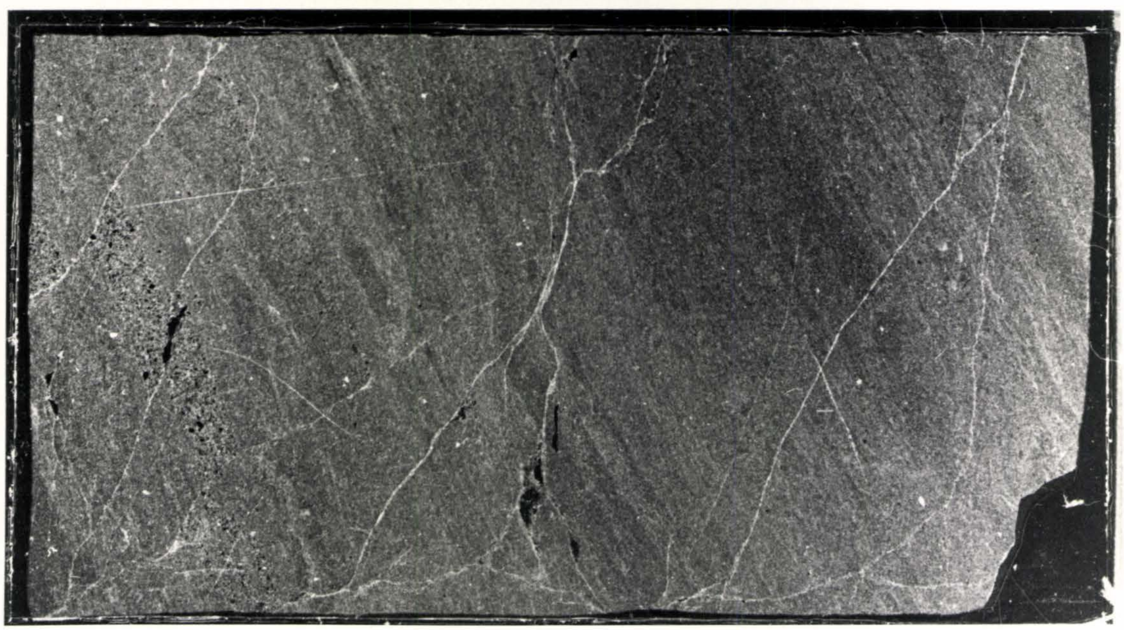

2) equal angles had to contain an equal number of fractures.

The fractures have the appearance of being emplaced very early in the rock's history, certainly prior to lithification.

2.3.1 Methodology

The fractures were measured from 11" by 14" photographs. Each photograph showed an entire slide. Magnification therefore ranged from 8.5-10. The photographs were negative prints, and the slide was illuminated by a point light source. This enhances the contrast in relief between the fracture and the medium. The fractures were measured directly from the photograph and reduced to their real length. Gradual gentle curving fractures were measured as a single fracture with an overall estimated orientation. Distinct orientation changes of more than 5^{o} on straight fractures were recorded as two distinct fractures. A total of 236 fractures were measured from 8 slides.

2.3.2 Results

The length of all fractures against orientation is is plotted in figure 2.5. From this graph one can see that there is a larger number of long fractures with orientations roughly east-west. Since many fractures go off the edges of the slide, their true length cannot be determined.

Figure 2.5 A plot of length of fractures vs. orientation. Fractures are measured from 90^{o}W to N to 90^{o}E only.

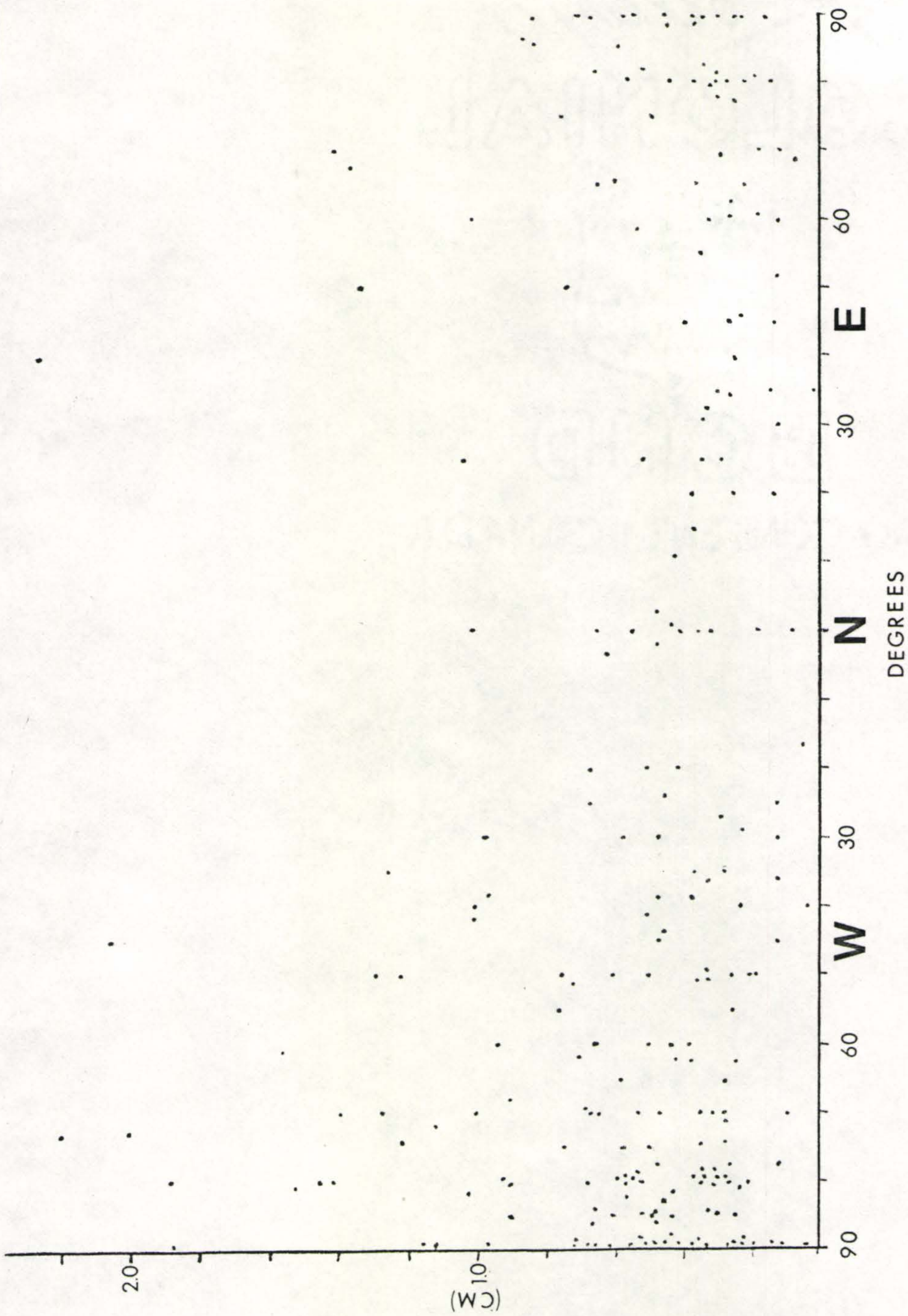
2.0
1.0
(CM)
90
60
30
30
60
90
W
N
E
DEGREES

Since there are fractures of almost all orientations one can say that fracture orientation, even though there is now a strong preferred orientation, was essentially random. Only a random original distribution would produce a full spectrum of orientations after deformation. It is therefore clear that condition 1 is met.

Plotting the number and orientation of the fractures on a rose diagram shows a strong preferred orientation (figure 2.6). Since the fractures are rotated into the λ_1 direction, one can set a λ_1 direction of roughly east-west and a λ_2 direction of north-south. Since the orientation is slightly bimodal a switch in λ_2 direction from 0^o to 10^oeast may have taken place.

Fracture orientations are plotted at 5^o intervals; the number of fractures per 5^o interval in this case equals 6.55 fractures. In a pure shear situation fractures having an original orientation of close to the presumed λ_2 direction are not rotated at all or rotated only small amounts. The two 5^o interval of $0^o \pm 5$ contain 6 fractures each. This is very close to the predicted value and implies the following:

1) The original distribution of fractures was random and

2) originally equal angles contained an equal number of fractures.

Figure 2.6 Rose diagram of 236 fractures, measured from 90°W to N to 90°E. The numbers are repeated for 90° to 270° in order to show a full range. The number of fractures are plotted in 5° intervals.

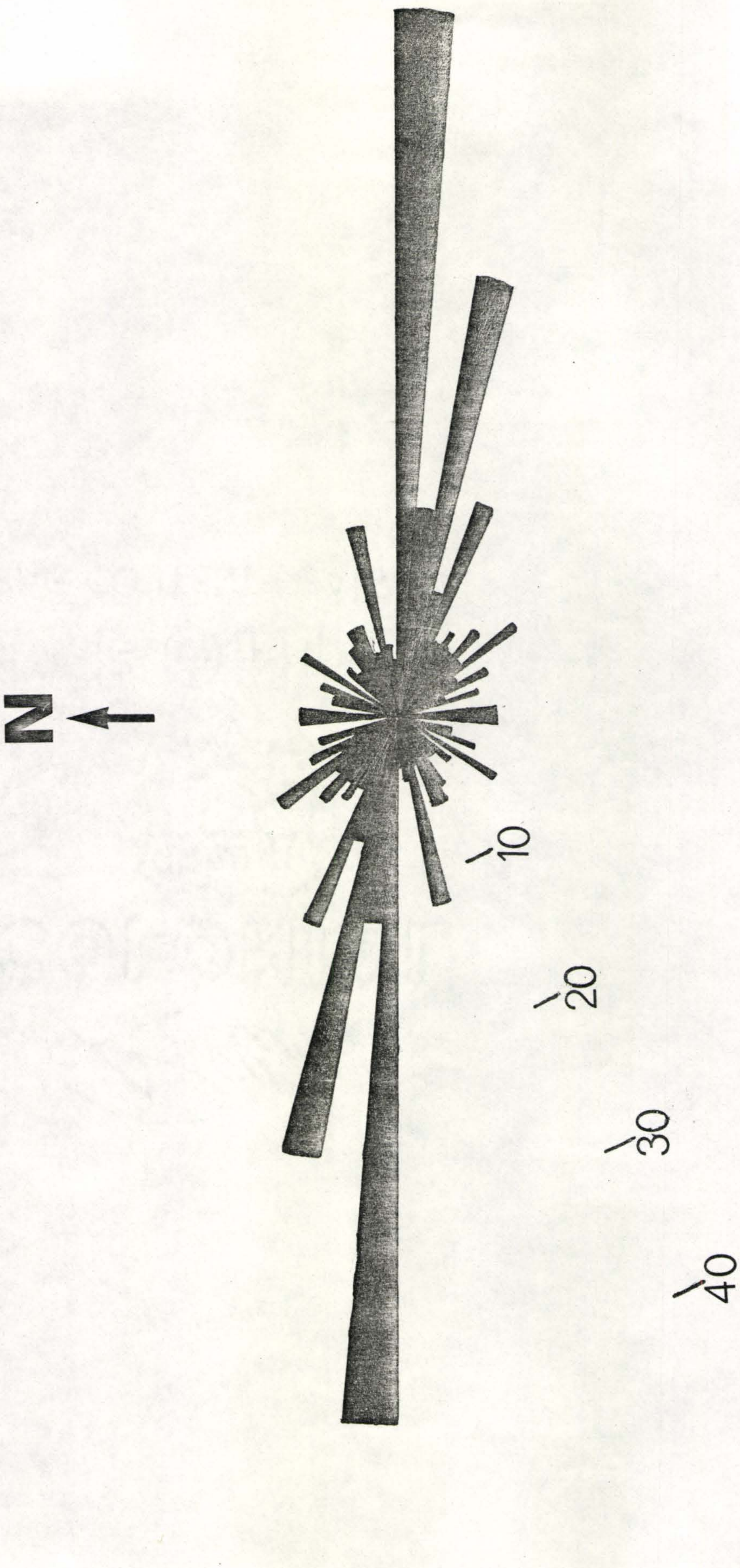
N
10
20
30
40

3) The deformational field was that of pure shear or very close to it.

4) 0^{o} is the λ_2 direction and the fractures were rotated very little or not at all.

2.4 Strain Estimates

In this sample the fractures and fractured and elongated clasts are used for strain estimates. All of the strain estimates used only give values for two dimensional strain and are only minimum estimates.

2.4.1 Fractures

We have seen that the initial distribution of fractures was random. Sanderson (1977) provides a method of determining the finite strain using lines with an initial random orientation:

"The frequency (F) of a uniform distribution of lines in a sector subtended by an angle α is:

$$F = \frac{n\alpha}{2\pi} \; (0 < \alpha \leqslant 2\pi)$$

where n is the total number of lines. For a uniform distribution, F is independent of the orientation of the sector and the frequency distribution is:

$$\frac{dF}{d\theta} = \frac{n}{2\pi} = \text{constant} \qquad (1)$$

If this initial uniform distribution is subject to a homogeneous strain, then the angle a line makes after deformation is given by:

$$\tan\theta' = R_s^{-1}\tan\theta \qquad (2)$$

where θ and θ' are measured from the maximum principal strain (x-axis), before and after deformation respectively, and R_s is the strain ratio,

$$R_s = (\lambda_1/\lambda_2)^{\frac{1}{2}}$$

The frequency distribution after deformation is given by:

$$\frac{dF}{d\theta'} = \frac{dF}{d\theta}\frac{d\theta}{d\theta'} = \frac{n}{2\pi}\frac{d\theta}{d\theta'} \tag{3}$$

From (2):

$$\theta = \tan^{-1}(R_s \tan\theta')$$

therefore:

$$\frac{d\theta}{d\theta'} = (R_s \sin^2\theta' + R_s^{-1}\cos^2\theta')^{-1}$$

giving:

$$\frac{dF}{d\theta'} = \frac{n}{2\pi}(R_s \sin^2\theta' + R_s^{-1}\cos^2\theta')^{-1} \tag{4}$$

This distribution, which I shall term the strain-modified uniform distribution, is symmetrical about a maximum when $\theta' = 0$ or π and a minimum when $\theta' = \frac{1}{2}\pi$ or $3/2\,\pi$.

The expected frequency (F) of lines in a sector subtended by θ'_1 and θ'_2 is given by:

$$F = \int_{\theta'_1}^{\theta'_2} \frac{dF}{d}\, d\theta'$$

$$= \frac{n}{2\pi}\int_{\theta'_1}^{\theta'_2}\left[R_s \sin^2\theta' + R_s^{-1}\cos^2\theta'\right]d\theta'$$

$$F = \frac{n}{2\pi}\left[\tan^{-1}(R_s \tan\theta'_2) - \tan^{-1}(R_s \tan\theta'_1)\right] \tag{5}$$

Since the data are drawn from a symmetrical, bell-shaped, distribution over the range $X \pm \frac{1}{2}\pi$, a natural approach would be to double the angles specifying the orientation of the lines and treat each as a unit vector in the range $(0, 2\pi)$. Vector addition will give a resultant vector (r) whose direction (θ_2) and magnitude ($|r|$) give suitable estimates of the mean direction and dispersion of the data. Calculation of $|r|/n$, where n is the sample size, provides a better statistic to describe the dispersion since it is normalized for sample size.

The purpose of introducing the parameters $\bar{\theta}_2$ and $|r|/n$ is to establish a simple means of estimating the strain ratio and orientation of the X-axis. Simulation of the deformation of both "ideal" and "random" samples from a uniform distribution has shown that $\bar{\theta}_2$ is a good estimator of the orientation of the X-axis. Since the strain-modified uniform distribution, after doubling θ', is symmetrical and unimodal, the resultant vector is a good estimator of both the mean and the mode of such a distribution and is independent of the origin of measurement of the angles, $|r|/n$ is found to increase steadily with increasing R_s and is approximately proportional to $\ln(R_s)$ for $R_s < 10$. The relationship between R_s and $|r|/n$ is found numerically and shown in [Fig. 2.7]." (Sanderson, 1977, p.200-202).

For the fractures $\frac{|r|}{n} = 0.715$. Going to figure 2.7 gives an R_s value of approximately 6.1 since:

$$R_s = \left(\frac{\lambda_1}{\lambda_2}\right)^{1/2} = \frac{(\lambda_1)^{1/2}}{(\lambda_2)^{1/2}} = \frac{1 + e_1}{1 + e_2}$$

Therefore:

$$\frac{1 + e_1}{1 + e_2} = 6.1$$

With the $R_s = 6.1$ known and the assumption of no area loss (volume loss in 3 dimensions) one can calculate the strain ellipse.

Known: $R_s = \left(\frac{\lambda_1}{\lambda_2}\right)^{1/2} = 6.1$ (6)

for no area change $\lambda_1 \lambda_2 = 1$ (7)

from equation (6):

$$\frac{\lambda_1}{\lambda_2} = 6.1^2$$
$$= 37.21$$

Substituting equation (7):

$$37.21 \; \lambda_1 \lambda_2 = 1$$
$$\lambda_2 = 0.1639$$

therefore: $\lambda_1 \; (0.1639) = 1$

$$\lambda_1 = 6.1$$

Figure 2.7 Relationship between $|r|/n$ and R_s for strain-modified uniform distribution. (after Sanderson, 1977)

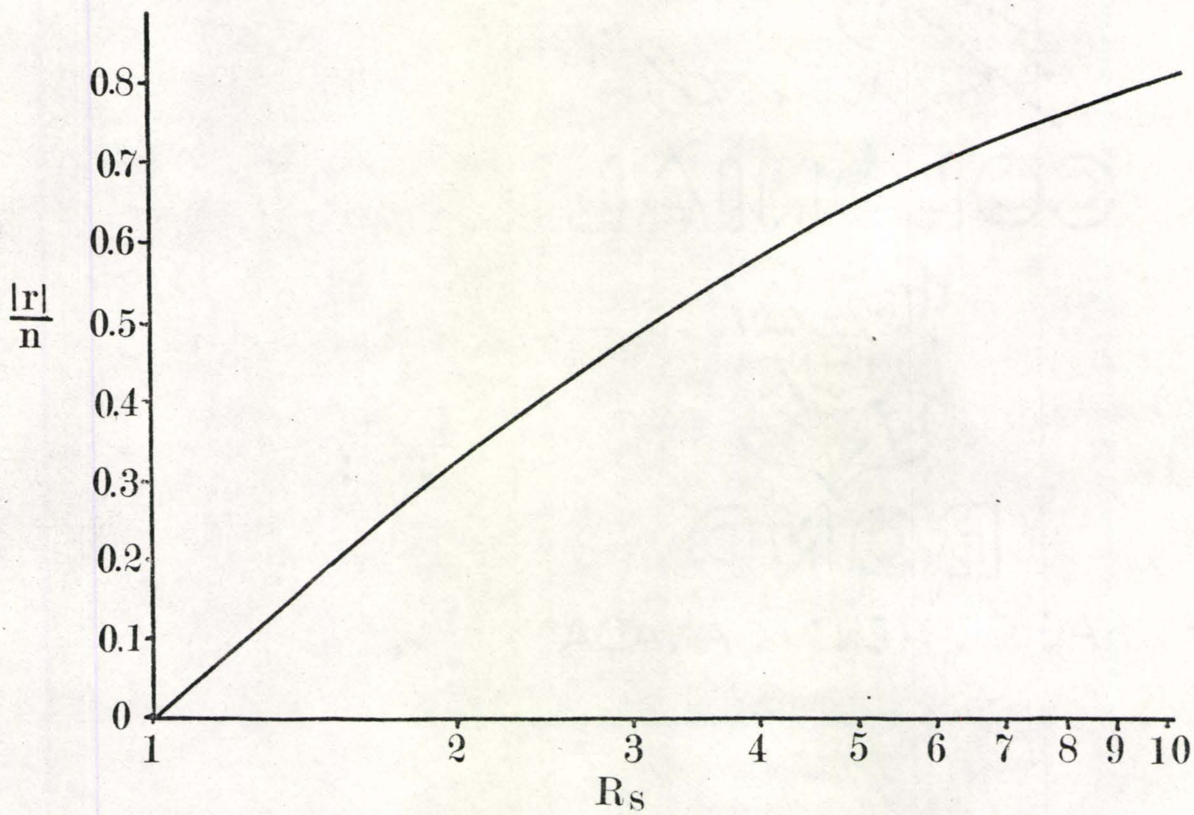
0.8
0.7
0.6
|r|
n
0.5
0.4
0.3
0.2
0.1
0
1
2
3
4
5
6
7
8
9
10
Rs

The axis of the strain ellipse relative to the original $|X|$ circle therefore are:

$$\frac{\sqrt{\lambda_1}}{\sqrt{\lambda_2}} = \frac{\sqrt{6.1}}{\sqrt{0.1639}} = \frac{2.47}{0.40} = \frac{1 + e_1}{1 + e_2} \qquad \begin{array}{l} e_1 = 1.47 \\ e_2 = -0.60 \end{array}$$

The strain ellipse is shown in figure 2.8. This is only the true strain ellipse if no volume loss occurred in the rock. The widespread effects of pressure solution however indicate that large volumes of water and possibly quartz were lost. The strain ellipse shown in figure 2.8 does therefore not represent the true strain ellipse. Since there is no way of calculating the volume lost, no accurate strain ellipse can be drawn. It can only be said that $R_s = 6.1$ represents a strong deformation and that e_2 may be an overestimate.

2.4.2 Clasts - Sample A

Sample A contains a number of clasts which have been fractured and extended in the λ_1 direction. The amount of extension can be measured and gives a minimum $1 + e_1$ value. In slide F03-2 a clast has been fractured. Calcite, growing parallel to the extensional direction, has filled in the fractures. Measuring the length of calcite and original clast material, parallel to λ_1, an extension $1 + e_1 = 1.6$ was determined, using the equation

$$e = \frac{\text{sum of length of all infillings}}{\text{sum of length of all original fragments}}$$

Another clast gave $1 + e_1 = 1.8$.

The clasts give minimum strain estimates from the

Figure 2.8 The strain ellipse with the corresponding original unit circle, assuming no volume loss. σ_1 direction is roughly north-south.

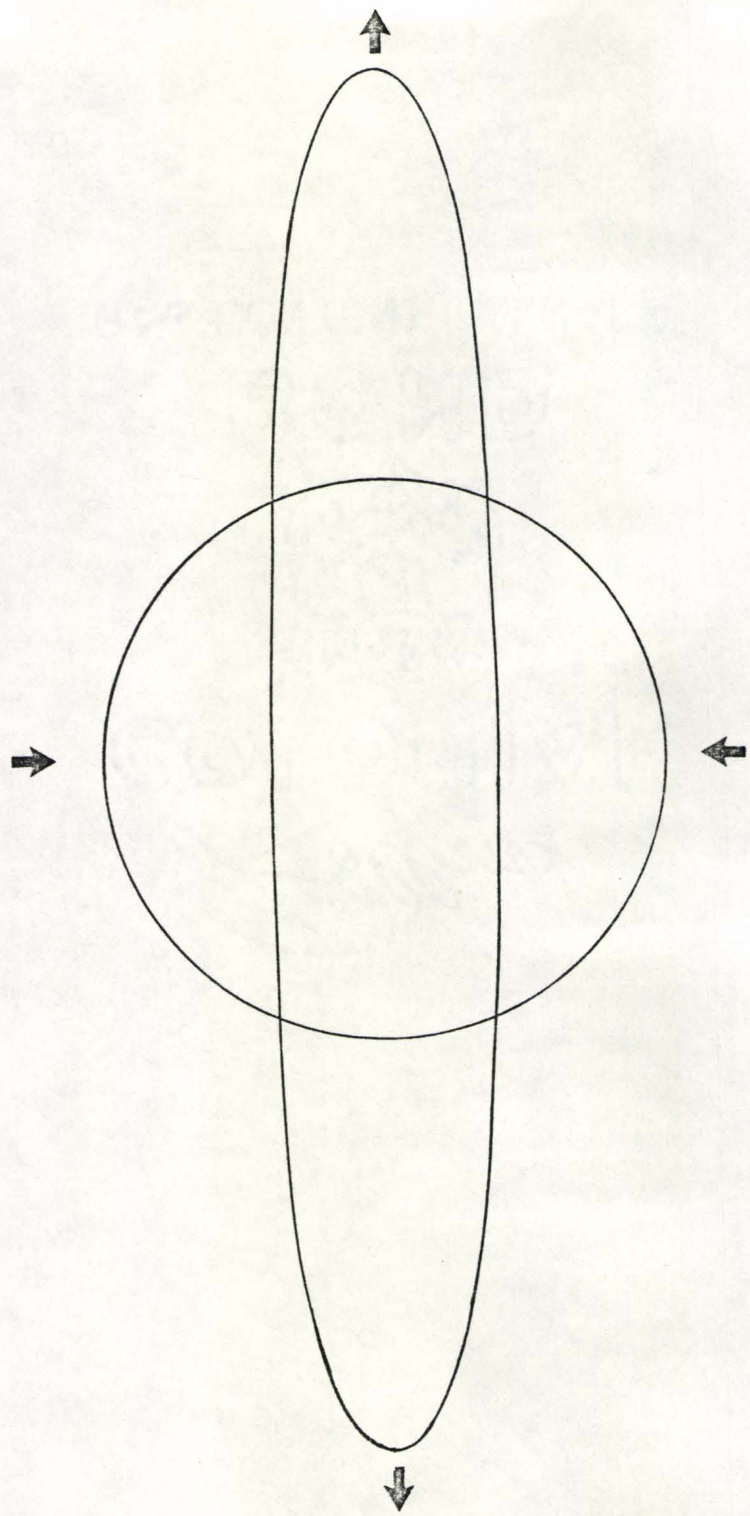

time at which the viscosity contrast between rock and clasts was small enough to induce fracturing in the clasts. It is not likely that this happened prior to lithification.

2.4.3 Conclusion

Since the rock has undergone volume change there is no way to relate the two strain estimates. The $R_S = 6.1$ value obtained from the fractures is more of a complete strain ratio than the value obtained by the fractures, because the fracture were affected earlier in the deformation than the clasts.

One can merely say that extension λ_1 is at least 1.8 and that the total strain ratio is at least 6.1.

2.5 Interpretation - Sample A

The fractures in sample A are interpreted as having been generated very early in its history, certainly prior to a part of the lithification process. The fracture pattern was originally random. The sample then underwent deformation. The orientation of the maximum principal stress axis σ_1 was approximately north-south and the stress regime was essentially one of pure shear. During the deformation the fractures were rotated towards $\sigma_2 = \lambda_1$

There is strong evidence for pressure solution in this sample. The variation of grain size described from slide F07-1 is thought to represent the effect of pressure solution. Other evidence for pressure solution is the flattening of coarse quartz grains against fractures as in slide F011.

Pressure solution shadows which formed at the north-south edges of the clasts (slides F08-18, F0-6, F08-2B, F07-3, F03), indicate that the more soluble quartz migrated away from these zones of high pressure. That there is no distinctive enrichment in quartz on the east-west edges, the areas of possible pressure shadows, proves that the quartz did not merely migrate from a high pressure zone to the nearest low pressure zone, but moved away from the immediate area of the clast. It therefore seems that quartz has been removed from the observed system. The fractures, which are of great abundance in this rock, may have formed convenient channels for this process. A plausible process might be as follows.

The "master" fracture, as described in slide F07-1, probably provided a channelway for the removal of quartz and water. "Feeder" fractures provide water from distal regions of the rock (areas outside the slide). In this way, with decreasing distance to "master" fracture the amount of water flushed through a unit volume of rock increased. This water dissolved quartz from the surface of all quartz grains in the area. Since the amount of water moved through each unit volume of rock increased with decreasing distance to the "master" fracture, the amount of quartz dissolved per grain is also likely to have increased in this direction. Such a process would explain the gradual decrease of grain size towards the "master" fracture.

The "master" fracture can be seen as an area of low stress, much in the way quartz rich layers are areas of low stress in rocks that have undergone metamorphic segregation. Quartz is then migrating from areas of relative high stress, the matrix, to the "master" fracture.

In slide F07-4 the large "master" fracture is roughly parallel to σ_1 . Here the "feeder" fractures approach the "master" fracture at high angles. The "feeder" fractures are therefore roughly parallel to the σ_3 direction. There are minor areas of pressure solution activity parallel to some of the larger "feeder" fractures. That these are not as extensive as in F07-1 is probably related to the difference in size between the "feeder" fracture in F07-4 and the "master" fracture in F07-1. In the "feeder" fractures of F07-4 the processes of movement of quartz towards relative low stress areas (as inferred for F07-1) seems to have operated the "master" fracture of F07-4. Being parallel to σ_1 however does not provide this gradient, since the quartz movement towards a low stress area has to be in the σ_1 direction and not at an angle to it. Since the "master" fracture is parallel to σ_1 , quartz would have to migrate obliquely to the σ_1 direction to enter the fracture. It poses no problem to move quartz at any angle to σ_1 in a fracture, presumably in solution. It does however seem unlikely that preferential movement of quartz obliquely to σ_1 would occur, unless the quartz is moving around an obstacle (ie. clast), since there is no incentive for such movement. That this is in fact the case may be demonstrated by looking at the areas along the "master" fracture, where no "feeder" fractures enter into the "master" fracture. Some of these areas show no indication of pressure solution activity, whereas others have a very thin layer, less than the thickness of the fracture, in which pressure solution micht have acted. This thin layer may be due to the fact that the "master" fracture is only roughly parallel to the σ_1 direction.

As mentioned above, the "master" fracture in F07-4 is one single large fracture. The "master" fracture of F07-1 is a bundle of fractures. The difference is related to their orientation. Because the "master" fracture of F07-4 was approximately parallel to σ_1 it was not rotated during deformation. Fractures of other orientations were rotated towards the σ_3 direction. That explains the large angle between the F07-4 "master" and "feeder" fractures. In slide F07-1 the "master" fracture probably had an original orientation close to the σ_3 direction. It was therefore rotated only by a small amount or not at all and "feeder" fractures of various original orientations were rotated towards the σ_3 direction and into near parallelism with the "master" fracture. This process, probably aided by the extensive pressure solution activity, accounts for the bundle-like appearance of the "master" fracture in F07-1.

During the deformation the fractures were probably fluid filled, making them ideal planes of weakness or miniature fault zones (slides F03, F07-4, F11). It is very likely that movement occurred along most fractures; but this cannot be determined for lack of correlatable features on opposite sides of the fractures.

During these stages of deformation the rock still has a very high fluid content and was probably poorly lithified. The viscosity of the clasts was very much higher than the viscosity of the rock. This caused the rock to deform by plastic flowing of matrix around the clasts, without fracturing them. The slightly bimodal distribution of the fractures in the rose diagram indicates a rotation of σ_1 or a second σ_1 of a later event. It is very likely that by the time of this later event the rock had been dewatered and lithified to a great extent. This increase in the viscosity of the rock decreased the viscosity contrast between matrix and clasts enough to cause tensional fracturing of the clasts. These tensional fractures infilled with calcite. The calcite crystals grew parallel to the principal extension direction (slide F03-2). The fact that only calcite and no quartz grew in these tensional openings indicates that the thermodynamic conditions in the rock had changed, making calcite the only freely moveable and locally depositable species. The main reason for the apparent lack of quartz movement may have been the lack of free pore water.

One can now divide the deformation of sample A into into three successive stages:

A) The rock is not yet fully lithified. Pressure solution is taking place using the fractures as channelways. The viscosity contrast between matrix and clasts is large, and the rock deforms by plastic flowage of matrix around clasts without fracturing them.

B) The viscosity contrast between matrix and clasts decreases enough to induce tensional fracturing in the clasts. Calcite, which is more soluble than quartz, grows in the tensional openings. Assuming that calcite is deposited due to a lack of free pore water, as argued above, then one may conclude that pressure solution activity involving quartz will have ceased prior to this stage.

C) The viscosity contrast between matrix and clasts becomes negligible. The rock is now essentially dry, and deforms plastically as a more-or-less homogeneous mass.

There is no evidence for retrograde metamorphism.

CHAPTER 3

3.1 Sample B - Description

Sample B, figure 3.1, shows a well defined cleavage in the hand sample. The spacing of the cleavage planes is on the order of 1-2 cm. A folded quartz vein, oriented broadly perpendicular to the cleavage, cuts through the sample. Where the cleavage intersects the vein the cleavage is bent.

On the microscopic scale the rock can be divided roughly into quartz rich and mica rich layers. There is a strong preferred orientation of mica flakes, whereas quartz grains are roughly equant and therefore show no preferred orientation. The grain size of the quartz is constant at a diameter of about 0.05-0.08 mm and most quartz shows no undulatory extinction.

The mesoscopic cleavage coincides with mica rich layers. The spacing of mica layers varies from 0.5 to 5 mm. The cleavage seen in the hand sample consists of wider bands of very closely spaced mica rich layers. In the thin section these wider bands are mica layers spaced close enough to show only gradual boundaries between each other. Outside the macro-cleavage (the wide bands) the mica layers have well defined sharp boundaries and their width is on the

Figure 3.1 Sample B. Showing the buckled quartz vein and cleavage planes visible with the naked eye. Along its longest edge the sample measures 25 cm.

order of less than 1 mm. Close to the quartz vein mica layers converge and the spacing of the mica layers increases as well (figure 3.2). Opaques are present throughout the rock but are concentrated in the mica layers. Grain size of opaques is larger than average in the mica layers.

Weak to relatively strong crenulation foliation is developed in mica layers. The degree to which the crenulation foliation is developed is roughly proportional to the thickness and intensity of the mica layer. The preferred alignment of micas is stronger in the mica layers than outside.

Towards the vein the spacing of mica layers increases as several mica layers join together, and approach the vein as one. The mica and quartz layers are therefore wider close to the vein than in the matrix.

Remnant bedding is visible and oriented roughly perpendicular to the cleavage. The bedding is gently folded and may be "offset" along mica layers. The bedding is on the millimeter scale and distinguished by alternating mica rich and mica poor beds. The mica rich beds do not contain nearly as much mica as the mica rich layers in the cleavage. The micas in the beds are oriented roughly parallel to the cleavage. Close to the quartz vein bedding is not as well preserved as in the regions away from the quartz vein.

Slide #3 (Figure 3.3) contains a feldspar clast. The

Figure 3.2 Slide A. Polarized photograph on top and point light source photograph on the bottom. Showing the buckled quartz vein. Cleavage is bent around the arcs of the vein.

A

Figure 3.2 Slide B. Polarized photograph on top and point light source photograph on the bottom. Showing the buckled quartz vein. Cleavage is bent around the arcs of the vein.

B

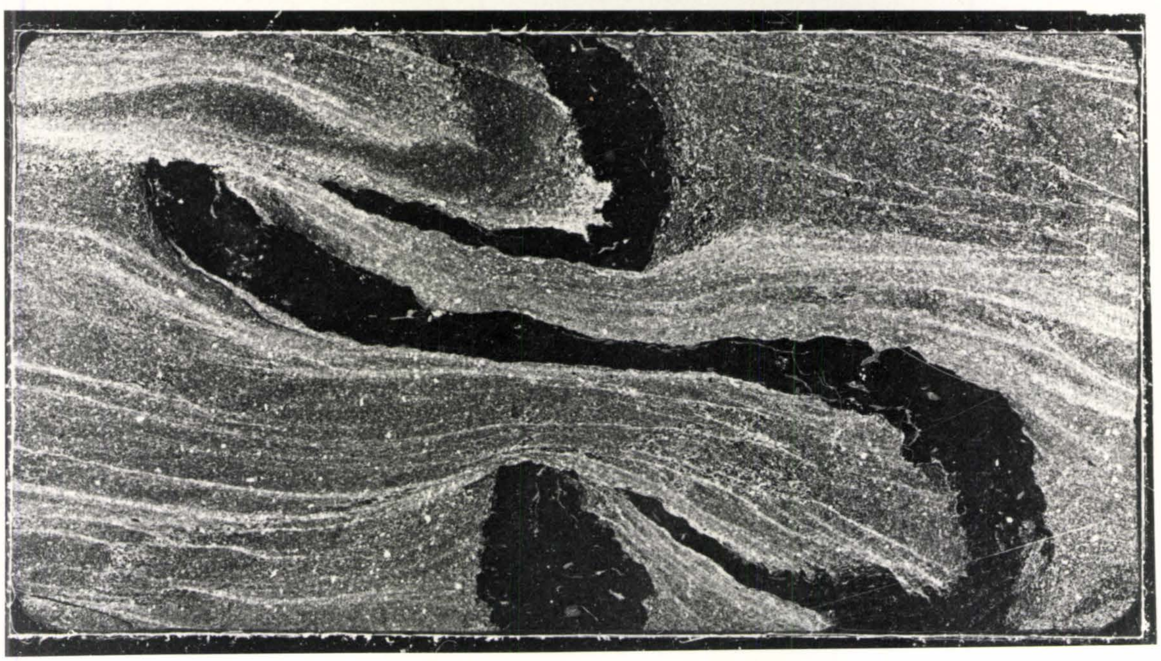

Figure 3.2 Slide C. Polarized photograph on top and point light source photograph on the bottom. Showing the buckled quartz vein. Cleavage is bent around the arcs of the vein

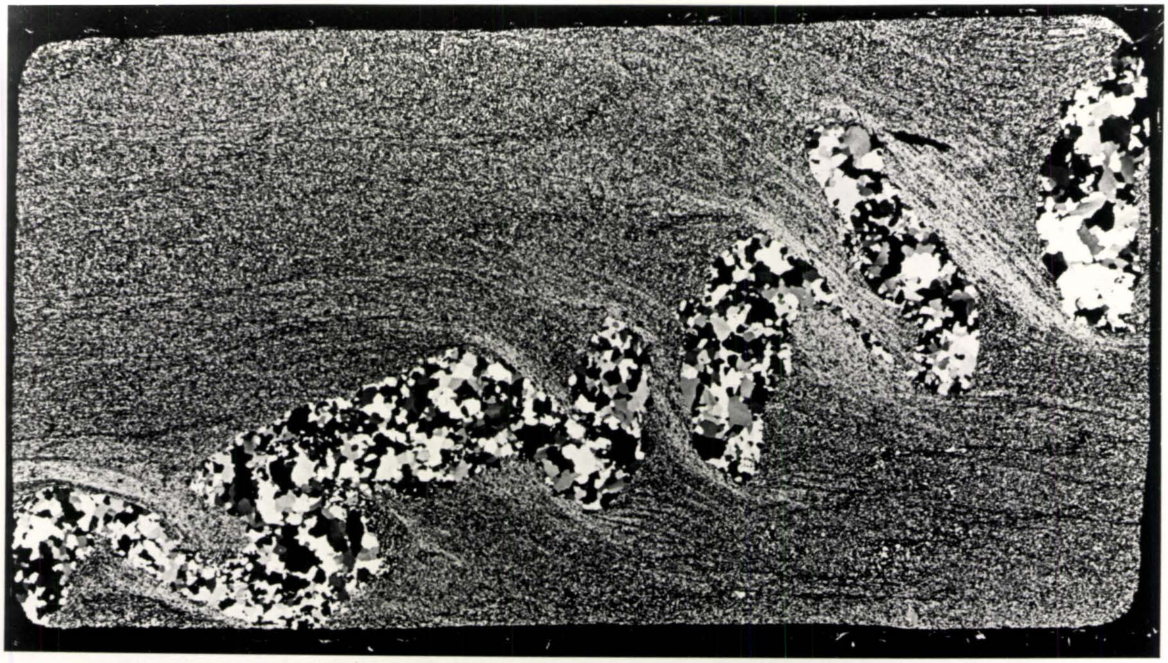

C

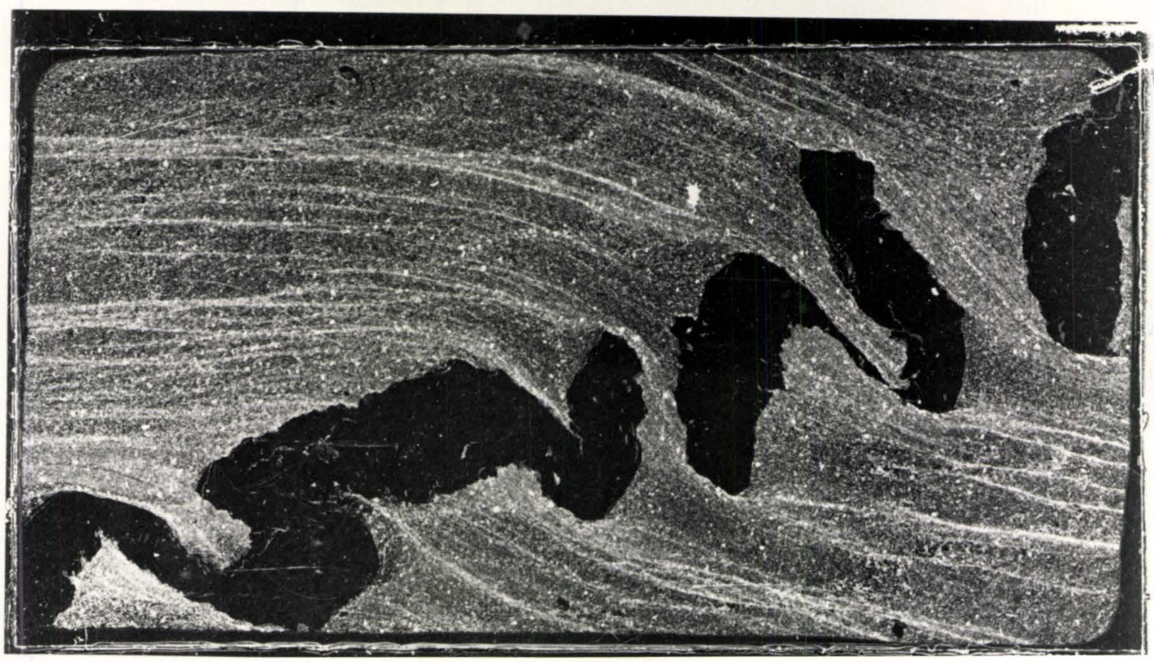

Figure 3.2 Slide D. Polarized photograph on top and point light source photograph on the bottom. Showing the buckled quartz vein. Cleavage is bent around the arcs of the vein.

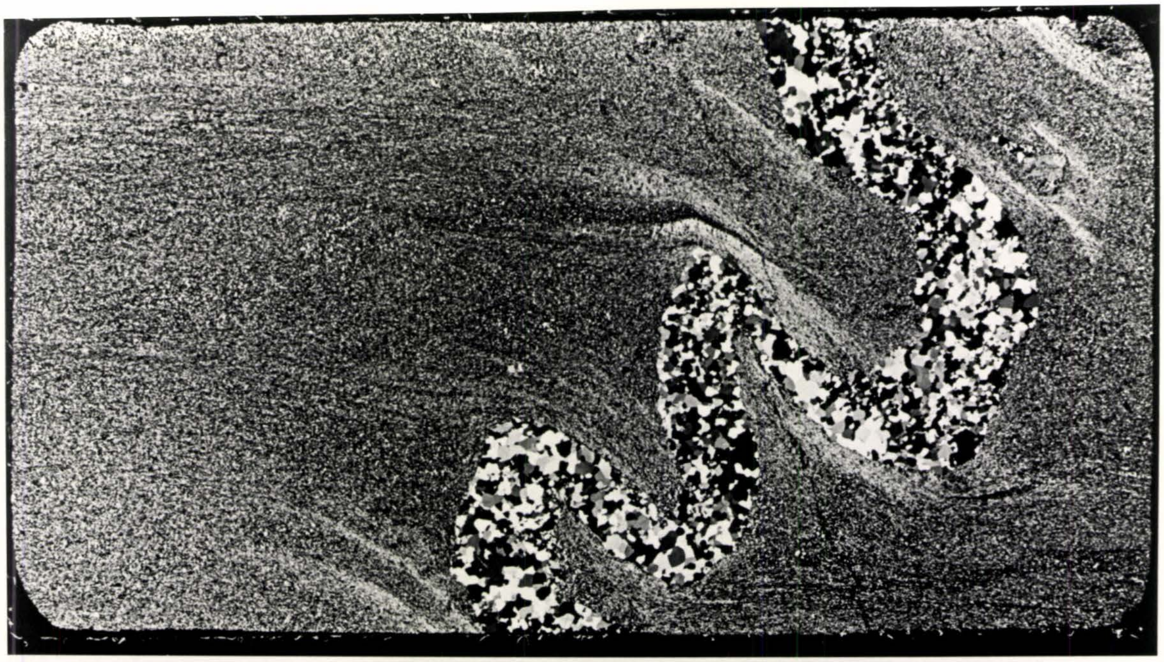

D

Figure 3.3 Slide 3. Polarized photograph on top and point light source photograph on the bottom. Showing the average microscopic cleavage spacing outside the contact strain zone. Cleavage planes bent around the clast. The The pressure shadow of the clast grades into a quartz rich layer. Remnant bedding, perpendicular to the cleavage planes is visible.

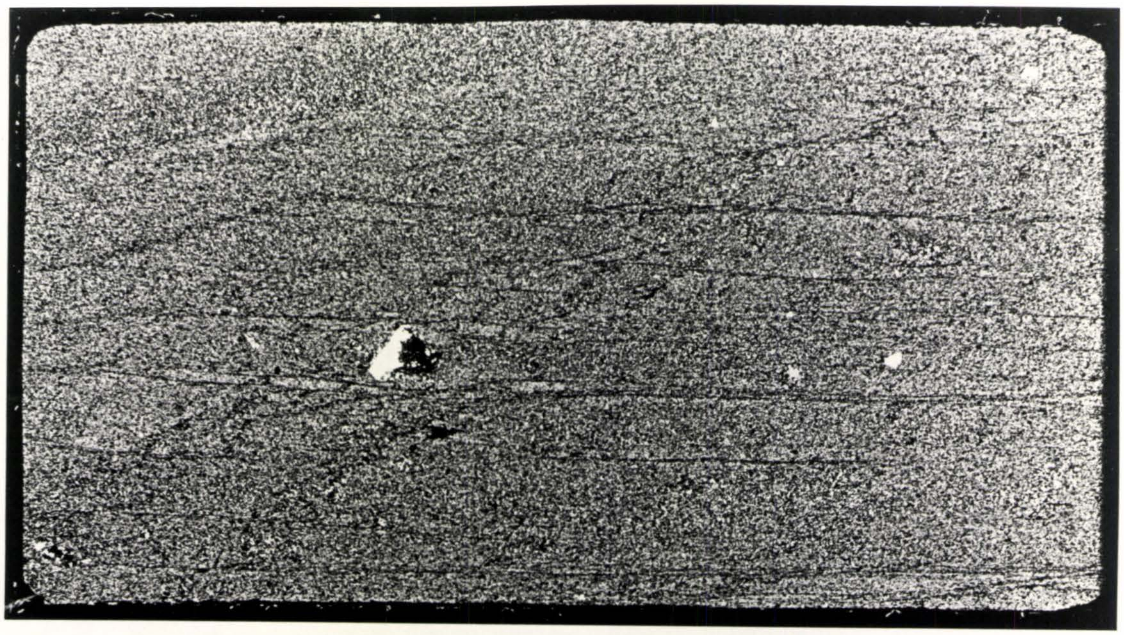

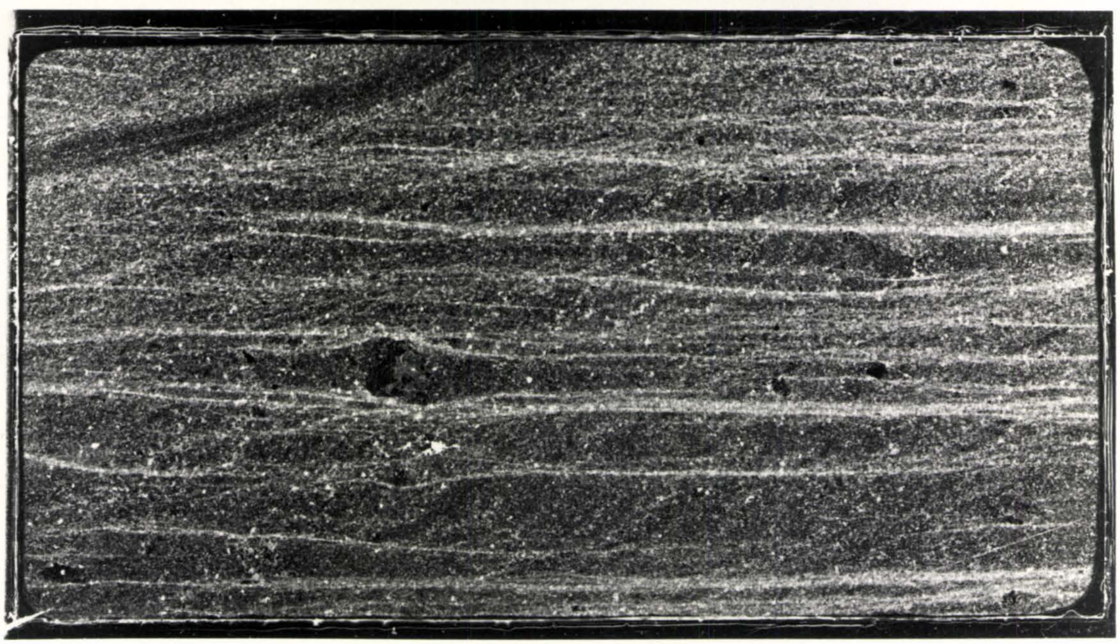

clast itself is strained and a pressure shadow has formed around it. The quartz in the pressure shadow is of larger grain size than the quartz in the matrix and it is strained. Mica is also present in the pressure shadow. It is aligned parallel to the cleavage and is of slightly larger grain size than the mica in the matrix. The pressure shadow grades into a quartz rich layer. Other clasts showed the same development.

The vein is composed almost entirely of quartz with only traces of mica. The quartz in the vein can be differentiated into two types. The first type is coarse grained, equant, has straight grain boundaries and shows no undulatory extinction. This type, the less common of the two, is mostly found in sections of the vein, that are fairly wide and straight or only gently curved. The second type of quartz has irregular to serrate boundaries, shows undulatory extinction and, on average, is of smaller grain size than the first type. This type is usually located in parts of the vein that are thinned or tightly bent (figure 3.4).

The boundary of the quartz vein is very well defined, usually by a layer of micas. In some cases pressure shadows form on corners of sharp turns in the vein. The quartz in these pressure shadows has the same appearance as that in the pressure shadows of clasts. At some sharp

Figure 3.4 Slide C showing a section of the quartz vein. The marked parts of the vein contain quartz predominantly showing serrated grain boundaries and undulose extinction.

bends in the vein a small bulge of quartz is located on the inside of the bend.

3.2 Quartz Vein Effects

Earlier we noted that cleavage behaviour close to the vein differs from that in regions far from the vein. This may be due to contact strain, induced by the deformed vein. We therefore examine a contact strain model, and compare it to sample B.

3.2.1 Contact Strain Model

In 1970, Dieterich produced a model of the distribution of principle axes of strain. He derived this distribution via a computer simulation of pure shear acting parallel to layering in a single layer in a semi-infinite matrix model. These results are displayed here in figure 3.5. From such a model, we may expect that cleavage would diverge from outer arcs, and converge in inner arcs of a folded layer in a semi-infinite matrix, if the bulk deformational kinematics are those of irrotational strain (equivalent to pure shear).

Ramsay (1967) notes that strain distributions in the inner arc areas yield class 3 folds, with isograms divergent as the limbs of the folds diverge. This agrees with Dietrichs model, but is difficult to show on a microscopic scale.

Figure 3.5 Buckled single layer model. Short lines are drawn perpendicular to the axes of maximum total compressive strain. (after Dieterich, 1969)

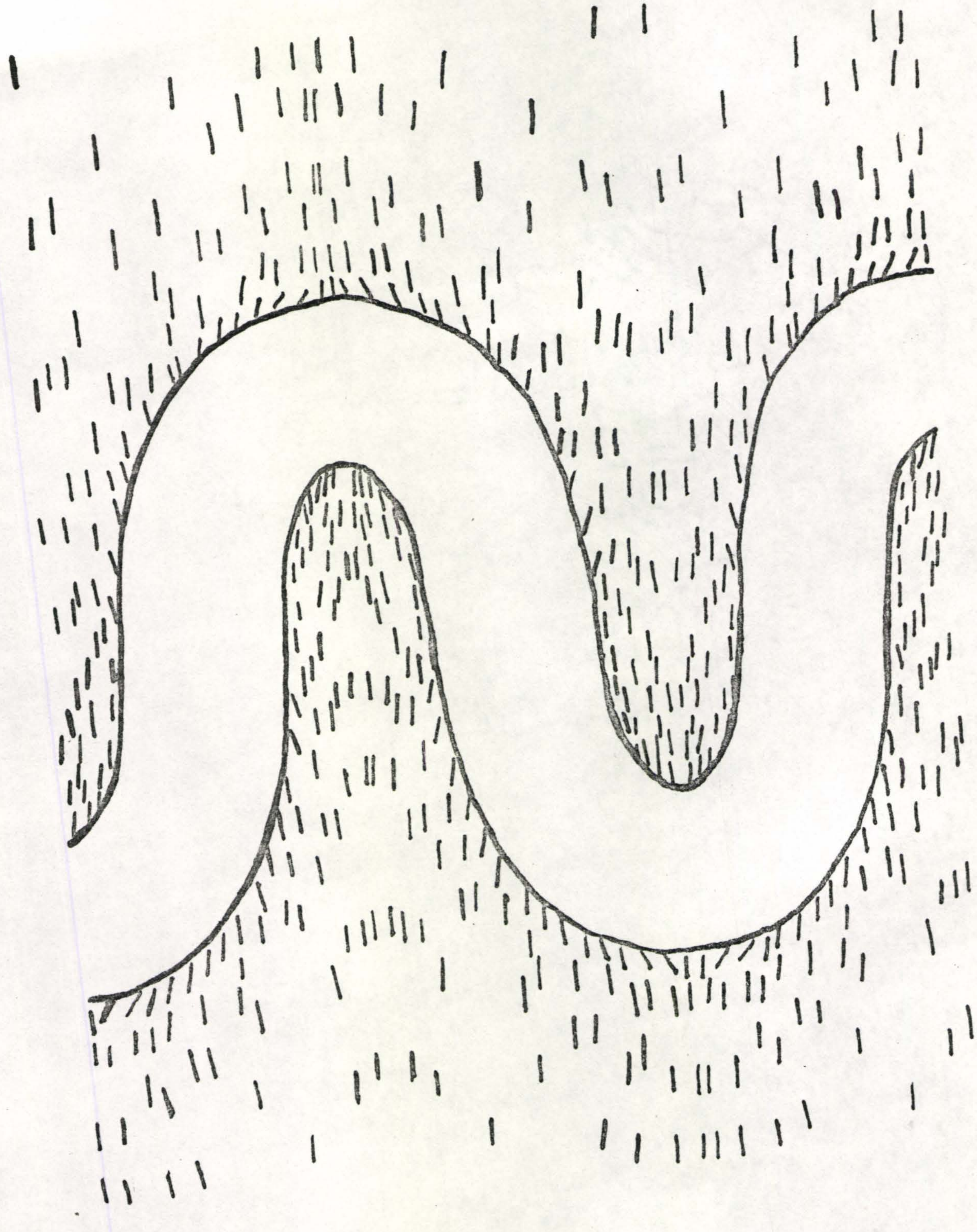

Theoretically, contact strain can extend infinitely for normal to enveloping surfaces. But for practical purposes, the contact strain effect is restricted to distances of the initial wavelength on either side of the buckled layer (Ramsay, 1967). Presumably, effects on cleavage should be equally restricted. Further finite neutral points are potential sites for deposition of "new"material.

3.2.2 Quartz Vein

In the thin sections figures 3.2A, 3.2B, 3.2C, 3.2D, it can be seen that the cleavage is diverted only up to distances of 2-3 cm on either side of the quartz vein. This is in the same range as the average wavelength of the vein. Cleavage fans around the outer arcs of the buckled vein and converges into the inner arcs of the vein. In some cases, example in slide B, quartz is located on the outer arcs of the vein in the triangle formed by the cleavage planes and the vein. This may be due to quartz crystallizing in the area of a finite neutral point. A more detailed comparison between cleavage in the immediate neighbourhood of the vein and in its far field reinforces the applicability of the model.

3.2.3 Methodology

Two slides were studied in detail, Slide A containing the vein and slide 1, taken approximately 8 cm away from the vein. Both slides were point counted in the following way.

A traverse across the slide perpendicular to the cleavage was made. For every step perpendicular to the cleavage, ten steps parallel to the cleavage were made. A sketch of this procedure is shown in figure 3.6 . Each step on the point-counter equals 0.27 mm. The number of quartz and mica (micas + oxides) grains for each line of ten steps parallel to the cleavage were recorded. This gives an accurate account of the percent variation of quartz and micas across the cleavage in the slide. The orientation of micas was also recorded.

3.2.4 Results

The number of quartz grains per step across the slide are plotted in figure 3.7. The cleavage coincides with the zones of high mica content. Generally the change from a quartz rich layer to a mica rich layer is very abrupt. Comparing slide A to slide 1 one can see that there are more stable plateaus as defined by the same quartz to mica ratio over several steps, in slide A, close to the vein. The range for the quartz percentage in the curve for slide A is less than for slide 1, never exceeding 70% and only rarely going below 30%. The overall quartz percentage in slide A is 40.8%, for slide 1, 43.5%.

Figure 3.8 shows percent mica vs. orientation of

Figure 3.6 Sketch of point counting procedure across cleavage. Each arrow indicates one point count (step).

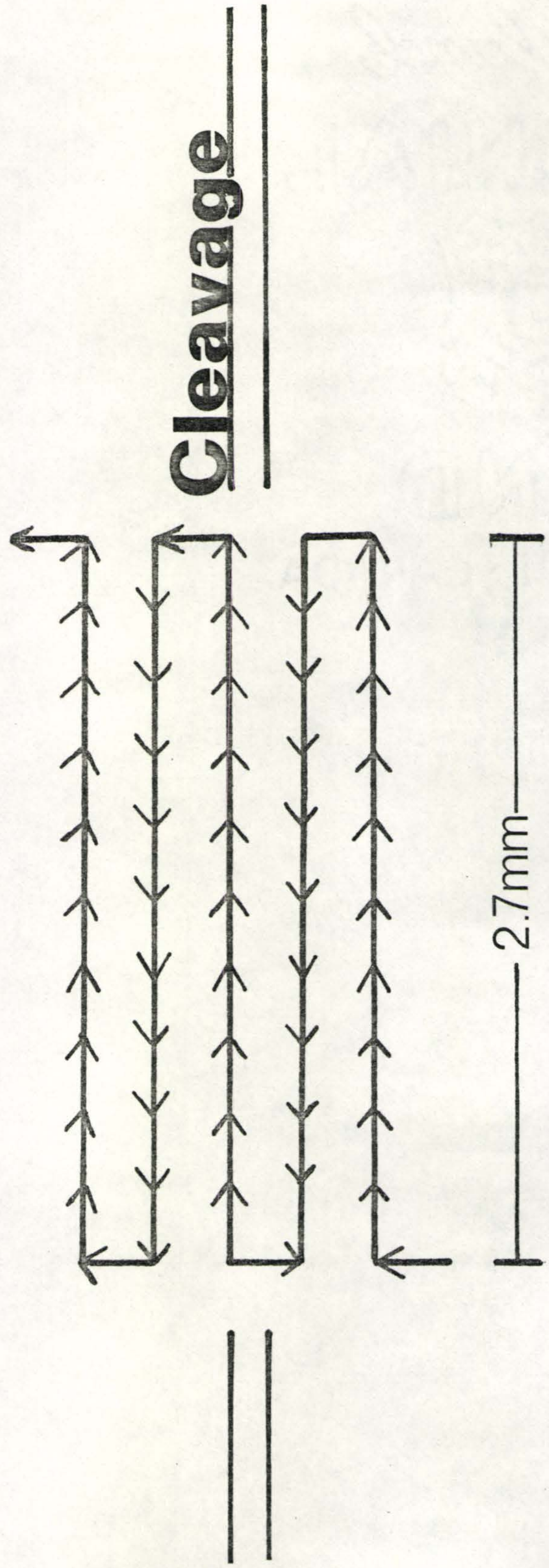
Cleavage
2.7mm

Figure 3.7 Results of the point counts across cleavage in slides 1 and A. Plotted are percentage of quartz per ten point counts vs. distance from the edge of the slide.

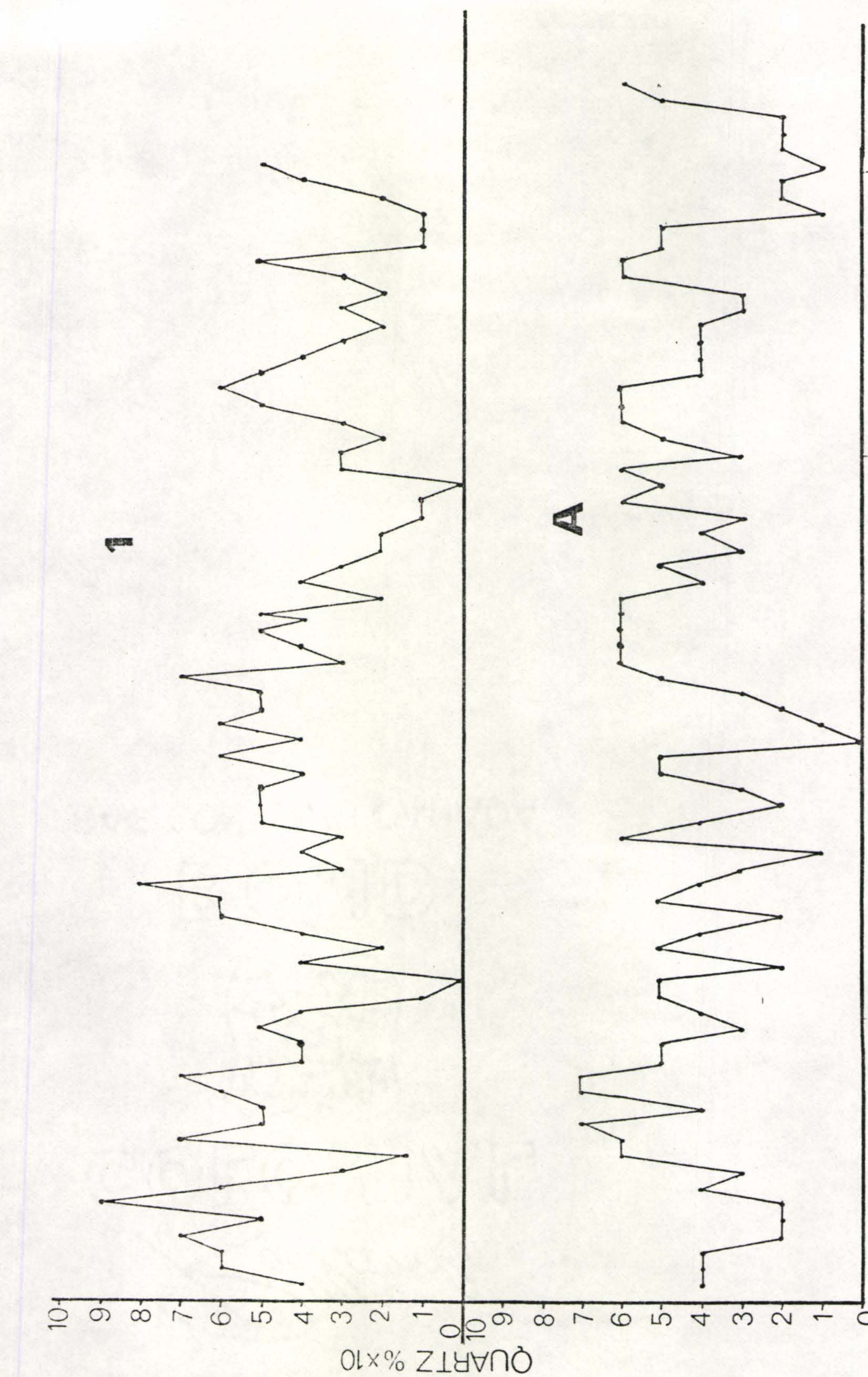
QUARTZ %×10
1
A
mm
0
5
10
15
20

Figure 3.8 Histogram of percent of total micas counted in each of slide A and 1 vs. orientation. Intervals are 5^{o}.

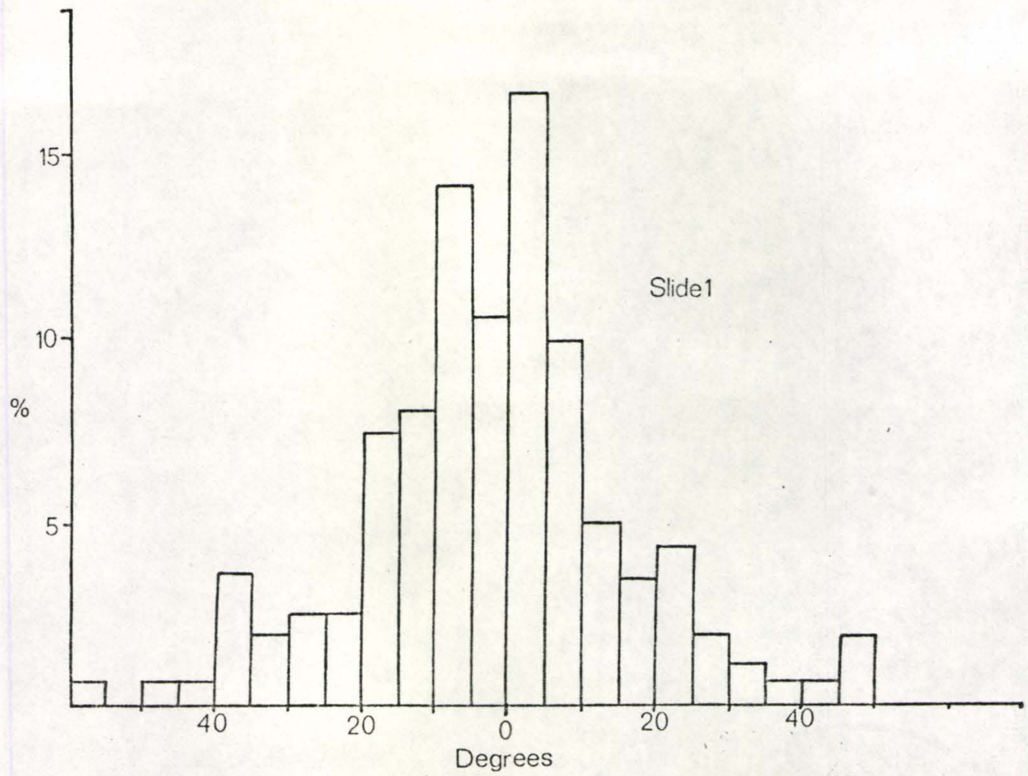
Slide1
15
10
5
%
40
20
0
20
40
Degrees

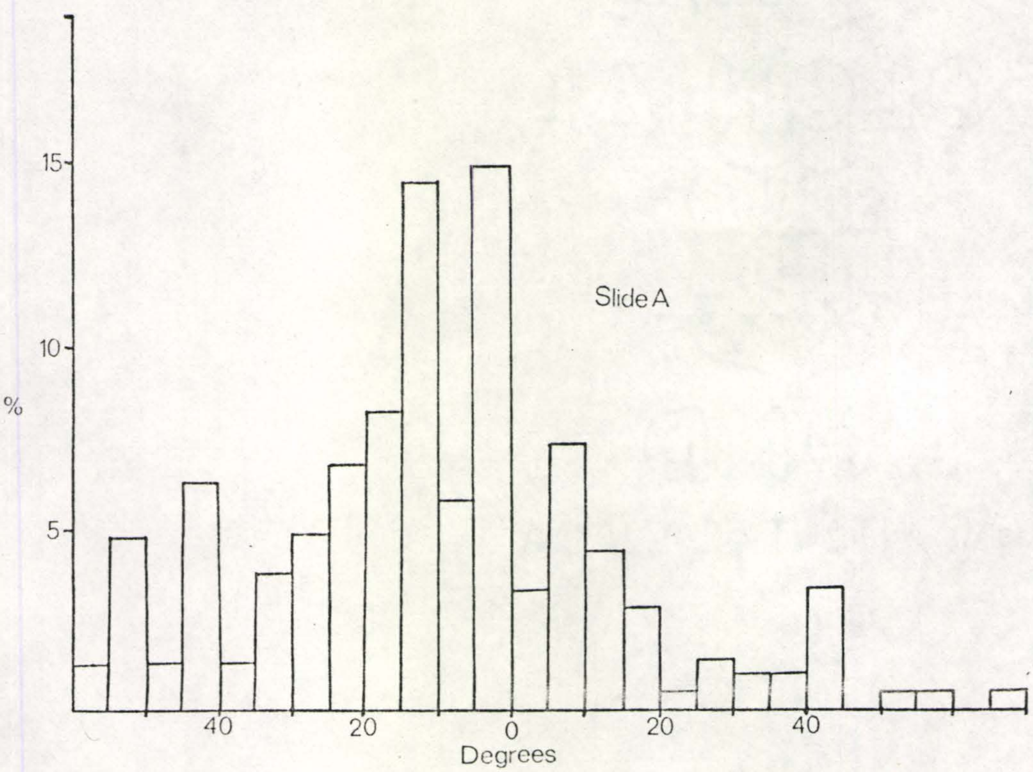
Slide A
15
10
5
%
40
20
0
20
40
Degrees

mica in slides A and 1. In slide A peak orientations of mica do not coincide with the cleavage (0^o), being instead a few degrees left hand of cleavage. In slide 1 the orientation distribution is roughly symmetrical with respect to cleavage.

3.2.5 Interpretation

In figure 3.7, slide 1, (far field) one can see four major zones of low quartz content, equivalent to cleavage. These are located at 2.43, 5.40, 13.77 and 17.82 mm. These can be divided into two groups which are separated by an 8 mm wide quartz rich band. The spacing between these zones in the groups is on the order of 2.97-4.05 mm. This may be interpreted as the characteristic spacing for major cleavage planes in the rock away from the vein. The reason for choosing the internal spacings in the two groups as the characteristic spacing is that in other slides, away from the vein, the predominant spacing, as determined by measuring of photos, is on the order of 2.5-4.5 mm.

In slide A, (near field) the area between 4.60 and 9.45 mm may be viewed as one thick cleavage plane. That it does not show a consistent low quartz value is due to the fact that it consists of several small cleavage planes, joining to form one wide band. Between 9.45 and 18.36 mm is a wide band of quartz, followed by a 1.62 mm wide cleavage band.

As stated above, cleavage planes join and thicken towards the vein. Close to the vein one can then say that cleavage bands are wider and spaced further apart than outside the contact strain zone. No numerical value can be assigned to this as other slides indicate that the spacing and width of the cleavage depends on the shape of the buckle.

The 2.7% difference in quartz percentage, between slide A and 1 is minor. It means that there is a total difference of 20 quartz grains counted between one slide and the other, out of a total of 760 (slide A) or 740 (slide 1) counts per slide. This seems to be well within experimental error. One can therefore say that the percentage of quartz is the same in both slides.

Figure 3.8 shows that both slides show a strong preferred orientation of mica. The mica in slide 1 shows a slightly stronger preferred orientation than the mica in slide A. This is probably due to two reasons:

1) The cleavage in the close proximity of the vein fans out, as predicted in the model. The bent cleavage would naturally lead to a wider range of mica orientation.

2) The vein actively reduces the stress in its close proximity. If one equates the degree of preferred orientation with intensity of stress, then the mica in slide A should be less oriented

in any one cleavage zone.

One can say that the model for contact strain agrees well with the behaviour found. The cleavage behaves in the way predicted and the effect is limited to a short distance from the vein.

3.3 Strain Estimates

The well defined cleavage and the extravagant folding of the quartz vein both indicate significant layer-parallel shortening. Similar folding is seen in the beds which flank the vein. We may use both sets of folds to estimate strain.

The basic method is simple (see Ramsay, 1967). Essentially we measure the length of the vein between two points and around the arcs, and compare this length (l_0) to the straight line distance between the two points (l_D) (figure 3.9). The shortening,

$$e_2 = \left[\frac{l_0 - l_D}{l_0}\right];$$

or expressed as a percentage

$$e_2' = \left[\frac{l_0 - l_D}{l_0}\right]100$$

When we do this for the vein and the bedding, we find that we have $e'_{2(vein)} = 68.5\%$ and $e'_{2(bed)} = 30\%$. The vein is dominantly of type 1B with near constant orthogonal thickness. So the shortening calculated is a good estimate for it. But the shortening in bedding is obviously not

Figure 3.9 Illustrating the difference between the folded length, L_O, and the straight line length, L_D, of the vein, used to determine strain.

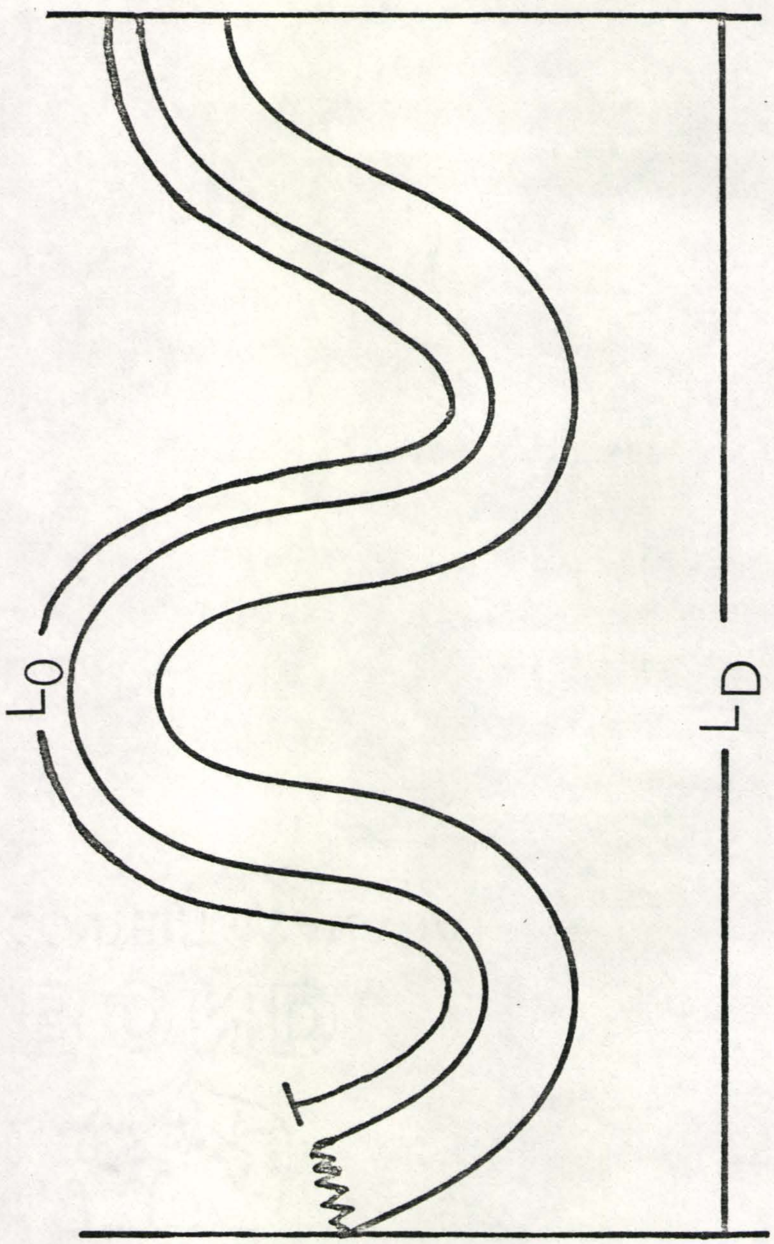
L_0
L_D

directly compatible with simple buckling. An explanation of the discrepancy lies in the degrees of viscosity contrasts as between vein and bed, and between bed and bed.

Many people, example Dieterich (1970) relate folding to viscosity contrast. In his scheme, a layer within a matrix in a system having a low layer-matrix viscosity ratio will deform largely by thickening, with only minor folding in a pure shear deformation. By contrast, a layer in a system having a high layer-matrix viscosity ratio will deform almost exclusively by buckling with no, or only minor, thickening in a pure shear deformation.

The viscosity contrast between the beds is relatively low they being essentially the same material. They deformed largely by thickening and only hinted folding. The viscosity contrast between the vein and the beds on the other hand, is quite high. Under stress, the vein therefore responded by buckling; thickening of the vein is negligible. The underlying assumption to this theory is that no volume has been lost from the rock. There is no evidence that anything other than water was lost, so this assumption seems to be justified.

The shortening value, given by the vein, is therefore a fairly accurate estimate of the two dimensional shortening the rock has undergone after emplacement of the vein.

3.4 Interpretations - Sample B

Since there is no evidence for a simple shear deformation in this sample, either in the vein or in the beds, it seems likely that the sample has been deformed in an essentially pure shear regime. Also the sample fits well the model used, which is based on pure shear deformation.

The segregation into quartz and mica rich layers indicates that extensive recrystallization has taken place in this sample. This is supported by the consistency in grain size, equancy and the lack of prominent undulatory extinction in the matrix quartz. It indicates that most of the quartz has been recrystallized. There is no evidence for removal of material by pressure solution out of the system. The almost consistent percentage of quartz away from and close to the vein shows that there is no depletion in quartz in the immediate vicinity of the vein. This leads to the conclusion that the quartz in the vein was derived from an outside source. It also means that the matrix quartz could only have been moved on a very limited scale. In order for the mica rich cleavage bands to form, quartz would have had to diffuse perpendicular to the cleavage. This leads to the conclusion that diffusion of quartz parallel to the axes of principal stress took place over greater distances in the contact strain region. Since mica rich bands are wider in this region quartz would have had to be removed out of wider areas and move larger distances to give the present picture. This may account for the fact that bedding is often unrecognizable in the contact strain region. The extensive recrystallization would have destroyed the fragile differences between beds. In the pressure shadows of clasts both quartz and mica are of larger grain size than in the matrix. The quartz in the pressure shadows often shows undulatory extinction.

This may be explained in the following way. Due to the low stress conditions the quartz crystallized to a larger grain size than in the matrix. Subsequent deformation strained the quartz but did not recrystallize it again. The pressure shadows grade into quartz rich layers, indicating that the low pressure areas of clasts act as nucleii for the quartz rich layers (Figure 3.3).

The quartz vein itself, being much more competent than the surrounding rock acts as a clast, creating a low stress zone in its immediate vicinity. This has a profound effect on the cleavage development. Close to the vein, the cleavage spacing is larger, and the cleavage bands are thicker than outside the area influenced by the vein. It may therefore be suggested that a higher stress regime leads to the formation of more closely spaced, thinner cleavage bands. However, it is likely that there is a number of complicating factors acting here, which invalidate the statement above. One of these factors may be that it is too simplistic to view the entire vein as one large stress reducer. Individual folds in vein will act as small clasts. Slide B is a good example of this. Here the "fold nose" of the vein extends about 1 cm into the rock. This acts as a clast that is quite large, yet smaller than the entire vein. A pressure shadow, containing quartz, has formed on the outward side of the fold nose, in the area of the finite neutral point. Such a large pressure shadow grades into a wide quartz rich band. The inside of the tightest fold is an area of higher stress. Since the quartz vein is much more competent than the surrounding rock, a tight folding of the quartz vein would have set up a local, very high stress field on the inside of the fold. Consequently the quartz in this area has been moved by pressure solution in the way described above into areas of low stress leaving a thick mica rich band which extends into the rock. The conclusion therefore is that the overall effect of the vein is that of a stress reducing "clast", yet the formation of the cleavage in the close proximity of the vein is very much affected by very local conditions set up by individual folds in the vein.

The strained quartz in the vein is produced by the deformation. Since the vein was very competent it would not have undergone much thickening, but would deform by buckling. As mentioned above, the strained quartz is located in areas of the vein that have undergone severe stretching or severe bending. The unstrained quartz on the other hand is located in areas that are straight and not obviously deformed. One can therefore assume that the unstrained quartz has not been affected by the deformation, and is therefore still in the same state it has been crystallized in originally. The quartz was therefore probably crystallized under equilibrium conditions. The strained quartz was strained during the buckling and is still in the same state. This implies that the quartz in the vein has not been recrystallized. In view of the extensive recrystallization that has occurred in the sample, probably at the same time as the buckling of the vein, this appears to be somewhat of a puzzle. A possible explanation may be that the thin layer of micas that in most cases rims the vein, effectively shielded it from the fluid necessary to dissolve and recrystallize the quartz.

The crenulation cleavage in this sample is developed stronger in thicker mica bands. Crenulating of micas is a way of taking up strain. It can therefore be suggested that when the rock has reached a certain degree of segregation a new mode of taking up strain, namely crenulation, is initiated. It appears that this rock has been deformed under a deformational field of nearly pure shear. However, there may be small elements of simple shear. These may be accommodated without problems in most of the rock, with the exception of thick mica bands. Here small components of simple shear may lead to the formation of crenulation.

CHAPTER 4

4.1 Comparison and Discussion

There are obvious similarities and differences between sample A and B. These may be used to interpret some of the factors effecting the development of cleavage.

The similarities are the following:

1) Both rocks have roughly the same bulk composition and are fine grained.
2) They are part of the same formation and therefore of the same approximate age.
3) Both have experienced the same grade of metamorphism.
4) The deformational field seemed to have been one of almost pure shear for both rocks.
5) Both have undergone a large amount of strain.

The major differences are:

1) Sample A is highly fractured; there is no evidence for fracturing in sample B.
2) Bedding, when seen, in sample A is well preserved. The grains are angular to rounded, with undulatory extinction common in quartz. There is no evidence of recrystallization in sample A. The quartz in sample B is equant, rounded, shows very little undulatory extinction and appears to have been extensively recrystallized.

3) There is ample evidence for the removal of quartz by pressure solution out of the system in sample A. There is no evidence for similar removal in sample B. The quartz appears to have been moved and recrystallized into quartz rich bands, but there is no reason to assume that any of it has left the system ie. the rock.
4) Sample B shows metamorphic segregation into competent quartz rich bands and less competent mica rich bands. There is no evidence for this in sample A.

It appears that all the similarities related to the original state and the large scale deformations of the rocks. The question that should be asked is then:

Why, when taking the same type of rock and subjecting it to the same grade of metamorphism, and the same deformational field, does the end result differ so greatly?

In order to answer this, one has to ask: What is the initial difference between the two samples?

This may be arrived at by looking at the major differences. It appears that the fractures are the major initial difference between the two samples. The fractures appear to have been implaced before lithification had been achieved. Later, during deformation these fractures provided ideal channels for the removal of water and dissolved quartz from the rock. Judging from the appearance of master fractures this process was very extensive and large volumes of water certainly and possibly quartz are lost. It seems reasonable to assume that the rock of sample A lost more water at a faster rate during lithification than a similar rock without fractures. This leads to the conclusion that at any given time during deformation sample A was drier than a similar rock without fractures. It is likely that the fractures being zones of weaknesses, acted in this way until long after compaction. Since water is by far the most mobile phase in the rock it is likely that essentially all pore water was squeezed out of the rock during deformation. The metamorphic conversion of clays to micas produces water which would probably have been lost as well. As a result, sample A would have been much drier than a similar rock under the same conditions.

Since there is no evidence for fractures in sample B it seems safe to assume that they were never present. Undergoing the same deformation and metamorphism sample B too would have lost water, but at a slower rate than sample A. The end result at the height of deformation would be that sample A is much drier than sample B.

Since the grade of metamorphism is low it seems reasonable to place the height of metamorphism with or near the end of deformation. The maximum temperatures reached during metamorphism are 400-500°C. This is not near the melting point of quartz or mica. Dissolution of quartz by water therefore seems to be the most likely mechanism responsible for the metamorphic segregation in sample B.

Water, as residual pore water or water produced by metamorphic reactions must therefore be responsible for metamorphic segregation into quartz and mica rich layers. Quartz is dissolved, in the same way as it is in pressure solution, but instead of being transported out of the system it is merely moved into a low stress zone. These zones may be nucleated by clasts, as described in the previous chapter.

The following conditions for the development of metamorphic segregation in the present situation may then be stated.

1) The system has to be closed or nearly closed. Loss of too much water leads to the development of pressure solution, but prevents the formation of metamorphic segregation.
2) A certain amount of water has to be present.

Taking Robins (1979) suggestions that micas act as catalysts in the development of metamorphic segregation, one might modify it in this case to the extent that micas act as catalyst, in as far as their formation provides the water necessary to cause metamorphic segregation. This would not modify his graph (figure 1.2) since very quartz rich rocks and very mica rich rocks would still be competent. The minima for least competency of the rock is then given by a composition in which there is enough mica to provide the

the maximum amount of water to recrystallize the quartz, yet not enough mica to classify the rock as competent due to an almost pure mica composition.

Stating the same thing the other way around one could say:

Original textures and structures may be preserved throughout limited metamorphism, if the rock remains dry.

Obvious limits are partial melting and intensive tectonics.

References

Alvarez, W., Engelder, T., and Geiser, P.A. (1978). Classification of solution cleavage in pelagic limestones. Geology, 6, 263-266.

Beach, A. (1974). A geochemical investigation of pressure solution and the formation of veins in a deformed greywacke. Contr. Mineral. and Petrol., 46, 61-68.

Cosgrove, J.W. (1976). The formation of crenulation cleavage. J. Geol. Soc. London, 132, 155-178.

Dieterich, J.H. (1970). Computer experiments on mechanics of finite amplitude folds. Can. J. Earth Sci., 7, 467-476.

Durney, D.W. (1972). Solution transfer, an important geological deformation mechanism. Nature, 235, 315-317.

Engelder, T., and Geiser, P. (1979). The relationship between pencil cleavage and lateral shortening within the Devonian section of the Appalachian Plateau, New York. Geology, 7, 460-464.

Gray, D.R. (1978). Relationship of crenulation cleavage to finite and incremental strain. Geol. Soc. Amer. Bull., 89, 577-590.

Hobbs, B.E., Means, W.P., and Williams, P.F. (1976). An Outline of Structural Geology. Wiley, 571 pp.

Ramsay, J.G. (1967). Folding and Fracturing of Rocks. McGraw-Hill Inc. 568 pp.

--------, and Graham, R.H. (1970). Strain variations in shear belts. Can. J. Earth Sci., 7, 786-813.

Robertson, J.A. (1976). The Blind River uranium deposits. The ores and their setting. Ontario Div. Mines M.P. 65.

--------, and Card, K.D. (eds.)(1972). Geology and Scenery. North shore of Lake Huron Region. Geol. Guide Book #4. Ontario Div. Mines.

Robin, P.F. (1979). Theory of metamorphic segregation and related processes. Geochim. Cosmochim. Acta, 43, 1587-1600.

Sanderson, D.J. (1977). The analysis of finite strain using lines with an initial random orientation. Tectonophysics, 43, 199-211.

Sorby, H.C. (1863). Uber Kalkstein-Geschiebe mit Eindrücken. Jahrbuch F. Mineralogie, 801-807.

Trurnit, P. (1968). Pressure solution phenomena in detrital rocks. Sediment. Geol., 2, 89-114.